

# Electric Characterization of DNA

INAUGURALDISSERTATION

zur

Erlangung der Würde eines Doktors der Philosophie

vorgelegt der

Philosophisch-Naturwissenschaftlichen Fakultät

der Universität Basel

von

François Dewarrat

aus Attalens (FR)

Basel, 2002

Genehmigt von der Philosophisch-Naturwissenschaftlichen Fakultät auf Antrag  
von:

Prof. Dr. C. Schönenberger  
Prof. Dr. H. Bouchiat  
Prof. Dr. H.-W. Fink  
Prof. Dr. A. Engel

Basel, den 2. Juli 2002

Prof. Dr. A. Zuberbühler, Dekan

# Contents

<b>1</b>	<b>Introduction</b>	<b>1</b>
<b>2</b>	<b>The DNA molecule</b>	<b>5</b>
2.1	Biological role . . . . .	5
2.2	Applications of DNA . . . . .	6
2.2.1	DNA computing . . . . .	7
2.2.2	Sensors . . . . .	8
2.2.3	Artificial structures . . . . .	9
2.3	Charge migration . . . . .	10
2.3.1	Charge injection . . . . .	11
2.3.2	Direct approach . . . . .	14
2.3.3	Electric conductivity measurements on DNA . . . . .	17
<b>3</b>	<b>DNA as fiber</b>	<b>25</b>
3.1	Introduction . . . . .	25
3.2	Experimental preparation . . . . .	26
3.3	Conductivity measurements . . . . .	29
3.3.1	Influence of external parameters . . . . .	31
3.4	Conclusions . . . . .	38
<b>4</b>	<b>DNA as single molecule</b>	<b>39</b>
4.1	Hydrodynamic stretching . . . . .	39
4.1.1	Mechanisms . . . . .	39
4.1.2	Experiments . . . . .	41
4.1.3	Summary . . . . .	46
4.2	Electric field orientation and positioning . . . . .	48
4.2.1	Mechanisms . . . . .	48
4.2.2	Experiments . . . . .	52
4.2.3	Summary . . . . .	54
4.3	Conductivity measurements . . . . .	57

---

4.3.1	Electrodes on top . . . . .	57
4.3.2	Molecules on top . . . . .	58
4.3.3	Other parameters . . . . .	61
4.3.4	Controls . . . . .	65
4.4	Conclusions . . . . .	66
<b>5</b>	<b>Conclusion</b>	<b>69</b>
<b>A</b>	<b>Structuring Techniques</b>	<b>71</b>
A.1	Electron-beam lithography . . . . .	71
A.2	RIE and wet chemical etching . . . . .	72
A.3	Metal evaporation . . . . .	73
A.4	Example . . . . .	74
<b>B</b>	<b>Observation Instruments</b>	<b>77</b>
B.1	LEEPS . . . . .	77
B.2	SEM . . . . .	78
B.3	Fluorescence microscopy . . . . .	80
<b>C</b>	<b>Recipes</b>	<b>83</b>
C.1	DNA Fibers . . . . .	83
C.2	Hydrodynamic stretching . . . . .	83
C.3	Electric-field . . . . .	84
C.4	Staining . . . . .	84
	<b>Bibliography</b>	<b>85</b>

# Chapter 1

## Introduction

Miniaturization, especially of electrical components, aroused a great interest in the science of the last fifty years, on the one side because it can reveal phenomena that are unsuspected at macroscopic sizes, and on the other side because there is a strong demand from the technology in order to improve performances of devices. In this field, science and technology interact strongly one with each other, as the understanding of the new phenomena is required to improve miniaturization, and a good technology is also required to investigate new features. The science dealing with this area is called mesoscopic physics, i.e. between the microscopic world of atoms and the macroscopic world. At mesoscopic sizes, the wave nature of electrons cannot be neglected as it is for macroscopic samples, so quantum mechanics is necessary to explain the observed phenomena. A typical example is the Aharonov-Bohm effect, where the electric resistance of a conducting hollow cylinder periodically oscillates with the magnetic flux going through the hollow.

Nanoscience can be defined as the research concerned with physical objects for which the nanometer length-scale is essential. It involves then numerous fields of research, among then mesoscopic physics, since the size at which mesoscopic phenomena become visible is typically in the order of micrometers or below. Two approaches can be considered in order to fabricate nanostructures: the top-down and the bottom-up approaches (see Fig. 1.1), which were foreseen by R. P. Feynman in his famous talk "There's Plenty of Room at the Bottom" that he gave in 1959 at the APS meeting [1]. The top-down approach uses macroscopic tools to manipulate small objects, as a pantograph would do. Typical instruments used for this purpose are scanning electron microscope (SEM), scanning force microscope (SFM, also called

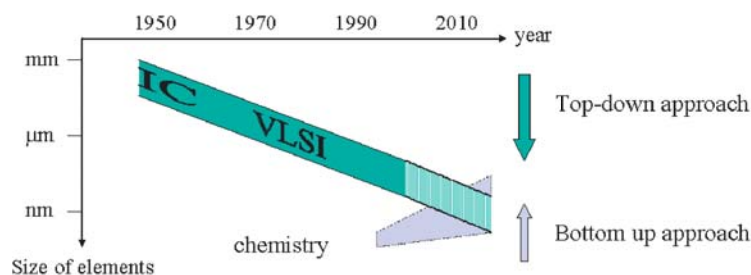


Figure 1.1: Top-down and bottom-up approaches used in nanotechnology. The size of the obtainable elements is shown as a function of time. (IC stands for Integrated circuits, VLSI for very large scale integrated circuits)

atomic force microscope, AFM) or scanning tunneling microscope (STM). The ultimate resolution goes up with improving technologies, even if the basics remain the same. Each structure has to be designed one by one, with the advantage that the process is well under control, at least within the resolution limit, but with the disadvantage that it can be slow. The other approach is called bottom-up. It uses basic construction bricks, atoms or small molecules, to assemble them in bigger structures or molecules, mostly by chemical processes. Once the parameters are established, this building process can be very fast due to the fact that the chemical reactions happen in parallel for all components. It is mostly probable that in the future, both techniques will be combined to make various kind of chips, from electronic components of computers [2, 3] to analyzing tools [4], and why not self-replicating nanorobots [5].

The DNA molecule (deoxyribo nucleic acid) might be an important actor on this scene, for several reasons, as explained in chapter 2. Among them is the questionable ability of DNA to support an electric current. The answer to this question can be of great interest either for fundamental understanding of the molecule itself, since it could have importance on repairing mechanisms after radiation damages [6], but also for an utilization on chip, as molecular wire or sensor.

The idea to use molecule in electronic device is not new. In 1974, A. Ratner already showed how to construct a simple electronic device (in this case a rectifier) based on the use of a single organic molecule. The molecular rectifier consists of a donor  $\pi$  system and an acceptor  $\pi$  system, separated by a  $\sigma$ -bonded (methylene) tunneling bridge. The response of such a molecule to an applied field is calculated, and rectifier properties indeed appeared [7].

The aim of this thesis is to characterize DNA's ability to support electrical current depending on the used strategy to prepare and measure it. Chapter 2 presents different aspects of DNA, from its functions designed by nature to other applications imagined by scientists. It presents also some models used to describe charge migration in DNA as well as a review of recent experiments and their different conclusions, since a precise and universal model cannot be presented. Chapter 3 and 4 describe the methods and results for the DNA device preparation and measurement, focussing respectively on bulk or single molecule properties. A description of the techniques used for the sample fabrication and observations is given in Appendix A and B. Appendix C contains the chemical recipes used for buffer or staining solutions with complete name and origin of the products.



# Chapter 2

## The DNA molecule

### 2.1 Biological role

It is obvious to everyone who observes nature that there must be a plan somewhere in the living entities. Trees make fruits out of which grow the same kind of trees, cats generate cats, and a lot of human babies inherit typical features of their parents. But the way nature can store this information was unknown for very long, and only in the 20th century one could explain the difference between the information that a living creature collects during its live (for example morphological modification or memories) and the one it gets from its parents. The question was "What kind of molecule can be stored in the cell, direct the activities of a developing organism and replicate itself with almost no loss of information?"

By the end of the 19th century biologists had recognized that the carriers of inherited information were the chromosomes, visible when the cell is ready to divide, but the fact that deoxyribonucleic acid (DNA) is the key substance came only later (studies on bacteria made in 1944, but commonly accepted since 1950) [8]. The reason why people had difficulties to accept DNA as the genetic support was the simplicity of its chemistry. A DNA chain consists of a long polymer composed of four subunits (nucleotide) containing the bases adenine (A), cytosine (C), guanine (G) and thymine (T), attached to the repetitive sugar-phosphate backbone almost like beads strung on a necklace.

In 1953, James Watson and Francis Crick could fit the x-ray diffraction measurements of the DNA to get the model of a double helix formed by the pairing of complementary bases (A with T and G with C) in the inside of the

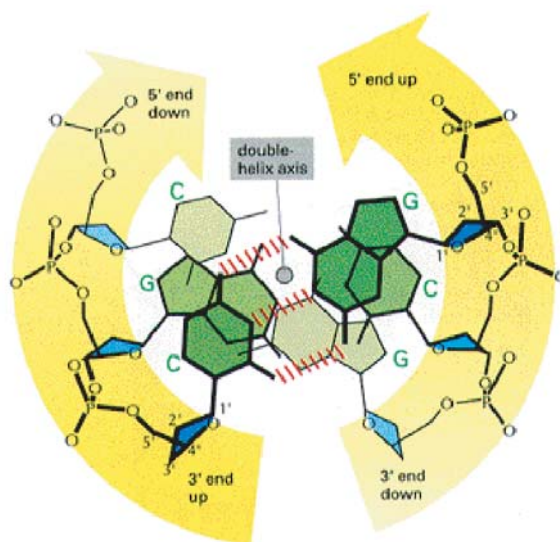


*Figure 2.1:* Axial view of the double helix, where one sees the stacking of the bases (here three G-C) and their hydrogen binding. [8]

helix and the sugar phosphates on the outside (see Fig. 2.1 and 2.2). Each base is covalently bounded to the backbone and bind to its complementary via hydrogen binding.

As a direct consequence of the base-pairing mechanism, it is clear how DNA carries information by means of the linear sequence of its nucleotides: different sequences carry different messages, and each strand can serve as a template to build a new complementary strand. The basic recipe to duplicate a double strand consists to open it and to build the complementary of each single strands, ending with two copies. The base-pairing mechanism is also used to produce chains of amino acids via the cell element called ribosome, since different sequences of three bases define different amino acids.

## 2.2 Applications of DNA

The base-pairing mechanism, a key property of the DNA, suggested to people to use the molecule for other applications than its biological role designed by nature. A common point between those is that they all require the storage and recognition of information, something that DNA is particularly suitable

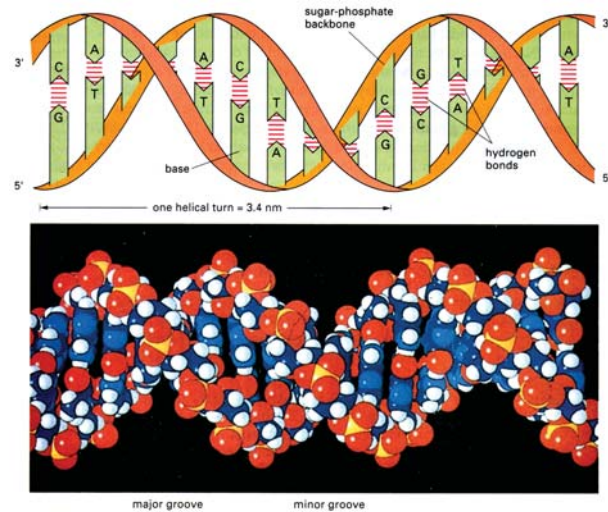


Figure 2.2: Double helix in B-form, schematic representation (top) and space-filling model (bottom) [8]

for.

### 2.2.1 DNA computing

One of these applications is the so-called DNA computing, originally proposed by Adleman [9]. It uses pieces of single DNA strands to code information and sort it out. An example of a problem solved by DNA computing is the so-called "salesman problem": a salesman wants to visit a set of cities, going through each one once and only once. The set of cities and their connecting paths are given, and the salesman has to find a way as it is defined above. This kind of problem is also referred as the Hamiltonian Path Problem. One of the algorithms to solve this problem is the following [9]:

1. generate random paths through the graph
2. keep only those that begin with the start city and end with the end city
3. keep only those paths with all cities
4. keep only those paths that enter all cities at least once

### 5. any remaining path is a solution

The key idea of Adleman is to use DNA single strands in solution to code the cities and the paths arriving at and leaving the city. Then strands with complementary parts to them, thus corresponding to a possible link between those cities, are added. The first point in the algorithm is achieved by the chemical binding reactions in the solution. The points two to four of the algorithm correspond to the extraction of the final product by bio-chemical methods such as amplification and filtering. If there is a solution to the problem, it comes out as a double-strand DNA, basically constructed from the different pieces corresponding to the cities and the links between them. In this experiment, the bio-chemical processes used to extract the solution are executed by the bio-chemist himself, requiring seven days of laboratory work. In more recent experiments [10], the overall process is autonomous and gets its energy from ATP (adenosine triphosphate), a standard energy provider in biology. The energy is released by the hydrolysis of ATP to ADP (adenosine diphosphate).

Theorists are still uncertain whether this kind of "calculations" has any future, and if yes in which circumstances. The advantage of the chemistry is that it is highly parallel, i.e. a lot of combinations between single strands are tested simultaneously, and the power consumption is quite low: 1J might be sufficient for  $10^{19}$  operations. The authors do not take into account the energy needed to produce the hardware, since it is also not taken into account with electronic computers. On another side, if the problem is getting so complex that one needs more than pico or micro mole to code all the nodes, then the size of a DNA computer will increase too fast. The question of error rate is also critical, as this kind of system is very sensitive to unprecise chemical reactions, if for example there is binding between two parts that are not fully complementary, leading to unusable results.

### 2.2.2 Sensors

Another application of the DNA's recognition mechanism is a sensor. The basic mechanism of a chemical sensor is a reaction between the sensor itself and the target. If the chemical to be detected is a single strand DNA, then nature gives already what the sensor has to use to complete the reaction: the complementary strand. Although the principle is very simple, the implementation of this reaction in a sensor that gives an output requires some

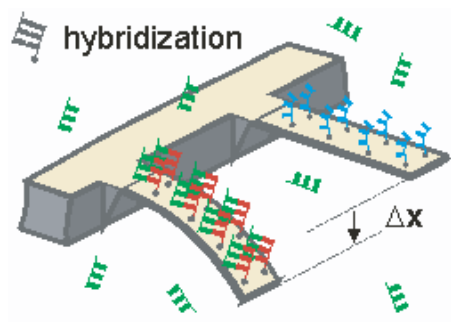


*Figure 2.3:* AFM cantilevers with detection system. Hybridization occurs on the cantilever that provides the matching sequence (red) to the nucleotide in solution (green), giving a differential signal  $\Delta x$ . [11]

cleverness. An example is given by the experiment described in [11]. Some single strands are attached to cantilevers (the same kind as the one used in AFM, see Fig. 2.3), and they are all dipped in the solution under test. If the complementary strand is present, it will bind to the attached one, thus producing some stress and a deflection of the cantilever. Unspecific binding bends the cantilevers in parallel, leading to no overall differential signal. The sensitivity is such that a single base mismatch can be detected for 12-mer oligonucleotides. Several tests can be made at the same time, and the sensor can be used several times if properly rinsed. Another advantage of this method is that the molecule under investigation does not need to be labelled. Applications in medicine, food industry or research are promising, and the authors estimate that the forces involved, around 1 nN, would be sufficient to operate micromechanical valves, with a possible application in nanorobotic machinery.

A different kind of DNA sensor is the one where the signal due to complementary binding comes out as a fluorescent signal or the cancellation of it. Some companies already sell the so-called DNA chips, like Affymetrix.

### 2.2.3 Artificial structures

Something different is the use of DNA strands as a construction kit. A careful design of the DNA sequences allows the fabrication of strands that form Y or T junctions, which can then be combined to build three-dimensional structures, such as a cube as shown in Fig. 2.4 [12].

Another possibility is to use DNA as a linker to beads, carbon nanotubes,

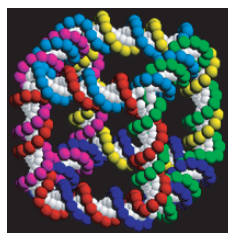


*Figure 2.4:* A cube whose edges are DNA strands. [12]

or even use it as a template for metallic growth. An example is shown in Fig. 2.5 from [13]: a gold particle is attached to a specific region on a single strand DNA (ssDNA). DNA can also serve as a template for a metallic growth [14]: a silver wire is chemically grown on a double strand DNA (dsDNA) placed between two gold electrodes. Several experiments show similar realizations with different metals [15–17].

## 2.3 Charge migration

It is necessary to be careful with the terms used to describe charge migration, because they refer to situations whose involved mechanisms and related consequences are different. Let's consider for example vacuum: electrons coming out a filament and accelerated move "without resistance", but it does not mean that the electrical resistance of vacuum is zero. When considering charges in a molecule, two approaches can be considered. In the first one, one injects a charge (hole or electron) in the system and then explores how efficiently or how fast this charge can be transferred from one site to another. This approach is typically performed by chemists, and the distances over which the migration of charges is investigated range from ångströms to few nanometers. The results of those experiments on DNA are in a reasonable agreement with theoretical models: they are presented in Sec. 2.3.1. In the other approach, one performs a so-called direct experiment: one measures the current as a function of an applied voltage, testing thus the mobility of the charges already present in the system. This approach, typically the one of physicists, is presented in the Sec. 2.3.2. At present time, no common picture can be presented for charge transport experiments over long distances in DNA. A brief review of different measurements is presented in the Sec. 2.3.3.

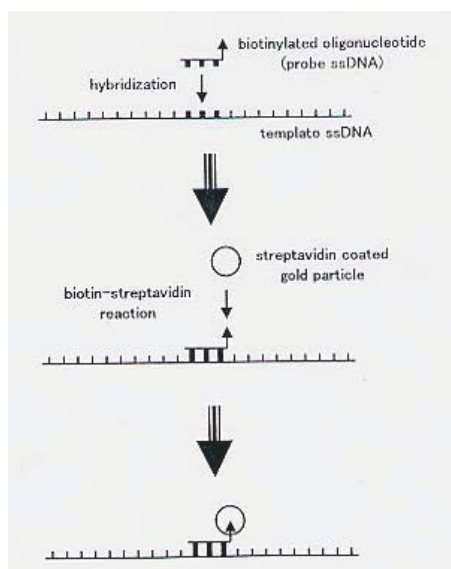


Figure 2.5: A two steps strategy to bind a gold particle to a template ssDNA. A biotinylated oligonucleotide is hybridized with the template ssDNA, then a streptavidin coated gold particle (5nm diameter) is bonded to it via a biotin-streptavidin reaction [13].

### 2.3.1 Charge injection

In 1997, based on several chemical experiments, Jortner presented two models to explain charge migration in DNA for a donor (d)- bridge ( $B_j$ )- acceptor (a) system [18]. One is a two-center unistep superexchange induced charge transfer  $d^*B_ja \rightarrow d^\mp B_ja^\pm$  (where  $d^*B_ja$  is the initial state with excited donor  $d^*$  and  $d^\mp B_ja^\pm$  is the final state with charge migration from donor to acceptor) and the other is a multistep charge transport with charge injection, charge hopping and charge trapping. A schematic picture of the two processes is shown in Fig. 2.6. The relative energies of the different states determine which process is occurring.

**Superexchange charge transfer** Electron hole transfer will occur for off-resonance coupling between the electronic origin and low vibronic states (in the energy range of  $k_T$ ) of the initial state with all of the  $d^\mp B_j^\pm a$  vibronic manifolds, with a large energy gap  $\delta E$ . Under this energetic conditions, superexchange-mediated electron transfer occurs with the rate

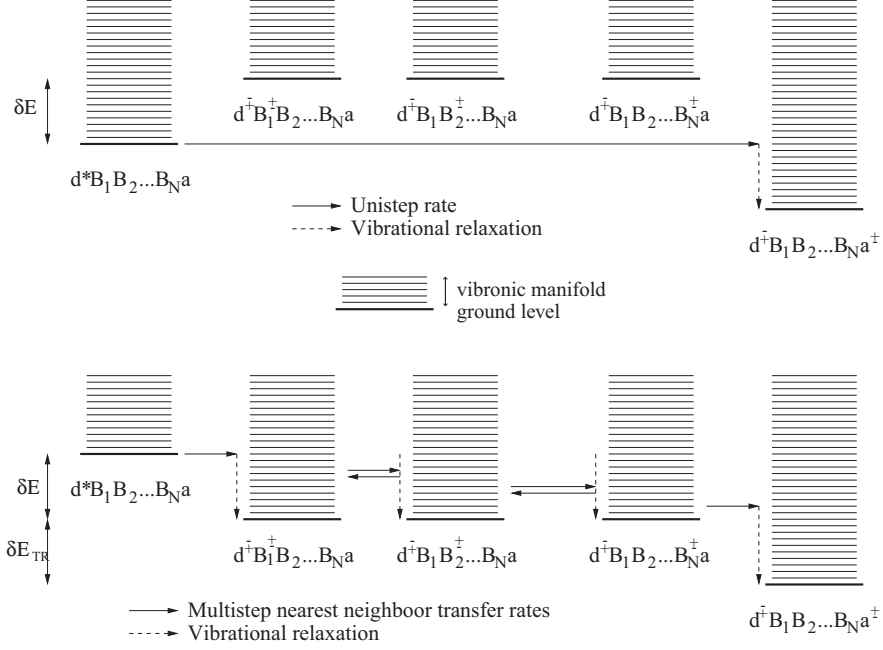


Figure 2.6: Level scheme for charge transfer via superexchange (above) and multistep charge transport via hopping and trapping (below) [18].

$$k \propto \exp(-\beta R) \quad (2.1)$$

where  $R$  is the distance between the donor and the acceptor.

**Multistep charge transport** Electron or hole transport will prevail when three energetic conditions are satisfied simultaneously (see Fig. 2.6):

- resonant coupling between the initial  $d^*\{B_j\}a$  state with the vibronic manifold of the primary ion pair  $d^\ddagger B_1^\ddagger B_2\dots B_Na$ , i.e. if  $\delta E < 0$ ,  $\implies$  injection of the hole/electron into the first base of the DNA
- near degeneracy of the origins of the vibronic manifolds of the ion pair states  $\implies$  charge hopping between the bases
- degeneracy of the base ion pair state  $d^\ddagger B_1B_2\dots B_N^\ddagger a$  and the ion pair state  $d^\ddagger B_1B_2\dots B_Na^\ddagger$ ,  $\implies$  charge trapping at the acceptor center

For an adequate description of the compound charge transport process, a specification of the individual microscopic rates for charge injection, hopping and trapping is required. Within a simple diffusion model, one would expect a charge transfer rate

$$k \propto 1/N^2. \quad (2.2)$$

If the degeneracy of ion-pair states is removed, typically with a bias<sup>1</sup>, the overall rate can be expressed as [18]

$$k \propto \frac{k_{hop}}{N^\eta} \quad (2.3)$$

where  $k_{hop}$  is the transfer rate of the hopping,  $N$  is the number of steps and  $\eta$  a parameter that depends on the ratio  $K = \frac{k_-}{k_+}$  (one for each direction) as follow:

- $K=1 \implies \eta = 2$  (i.e. without bias)
- $K < 1 \implies 1 \leq \eta \leq 2$  (acceptor direction-biased)
- $K \ll 1 \implies \eta \simeq 1$  (linear N dependence)
- $K > 1 \implies \eta \geq 2$  (for moderate K value, donor direction-biased)

For large values of  $K$ , the overall charge transfer rate has again an exponential dependance ( $k \propto \exp(N \ln K)$ ).

The variations of nearest neighbor electron coupling terms caused by zigzagging between bridge units across the two strands of DNA (or other disorder sources) have also to be taken into account when doing the calculation, however those effects will not change the fact that the distance dependence is weak (power law).

For charge transfer in proteins, the first mechanism (superexchange) is the dominant one, and for quite a long time, the debate was about which process occurs in DNA: only superexchange, or also multistep charge transport? Different values for  $\beta$  were presented:  $\beta < 0.2 \text{ \AA}^{-1}$  in [19] or  $\beta = 0.64 \pm 0.1 \text{ \AA}^{-1}$  in [20], whereas in protein  $\beta$  is typically in the range of 1 to  $1.5 \text{ \AA}^{-1}$  [21]. It was then pointed out that the parameter  $\beta$  can be used only if the energetics allow a coupling between donor and acceptor [22]. Finally, the affirmation

---

<sup>1</sup>Interactions with counterions can produce similar effects, as they can stabilize or destabilize the ion pairs with a large scale charge separation

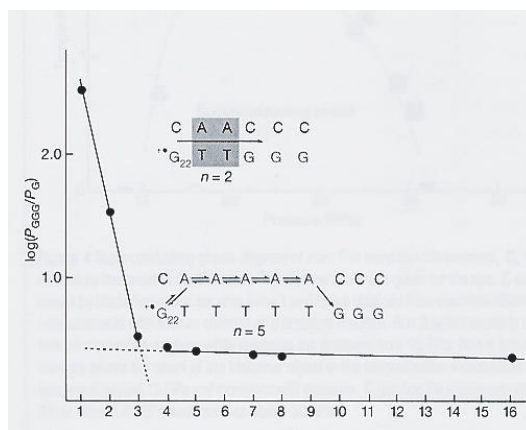


Figure 2.7: Plot of  $\log(P_{GGG}/P_G)$  as function of the number  $n$  of the AT base pairs. For  $n = 2$ , there is a superexchange charge transfer, whereas for longer distance (example with  $n = 5$ ), a A-hopping mechanism takes place. The first slope gives a  $\beta$  value of  $0.6\text{\AA}^{-1}$  [23].

of Jortner, i.e. the presence of the two mechanisms as presented above, has been recently verified for example by the group of B. Giese who performed the following experiment [23]: they first injected hole at a modified G base separated from a triple G by  $n$  AT base pairs. GGG plays the role of an electron donor, i.e. acceptor for hole, because it is more easily oxidized than a single G. The strand was then cleaved with a chemical treatment at the place where the hole was trapped. The ratio of the number of strands cut at GGG<sup>2</sup> (i.e. the hole went through the AT base pairs) and the number of strands cut at G (hole didn't move) as a function of  $n$  is proportional to the charge transfer rate. Their result is shown in Fig. 2.7, and is explained as follows. There is a coherent superexchange reaction (single step tunneling) with transfer rate following the Marcus-Levich-Jortner equation (Eq. 2.1) and a thermally induced hopping process (A-hopping), slightly influenced by the number of AT base pairs.

### 2.3.2 Direct approach

The basic physical approach about charge transport is to consider Ohm's law  $j = \sigma E$  (or its macroscopic version  $U = RI$ ). Drude's theory describes the conduction mechanisms considering that the electrons form a free electron

<sup>2</sup>They are called  $P_{GGG}$  as the chemical used for cleavage is piperidine

gas. The conductivity is then given by

$$\sigma = \frac{ne^2\tau}{m} = n\mu e \quad (2.4)$$

where  $n$  is the volume electron density,  $\tau$  the relaxation time,  $m$  the mass (or effective mass in the nearly free electron model) and  $\mu$  is the mobility defined as the ratio of the electron speed and the applied electric field. It is the solution of the equation of motion for the electrons steadily accelerated by the electric field and losing their speed by inelastic collisions every  $\tau$  seconds in average.

The conductivity  $\sigma$  varies from one material to the other over a very large range of magnitude: there is roughly a factor of  $10^{25}$  between the conductivity at room temperature of the best conductors, like copper, and the insulators, like quartz. It also depends, for most of the materials, on the temperature. A plot of conductivity as function of temperature shows a negative slope for metals and a positive slope for semiconductors or insulators, as shown in Fig. 2.8. Note that in metals the conductivity doesn't increase to infinite as temperature goes to zero, since the collisions responsible for the finite conductivity are not with phonons anymore as at higher temperature, but with impurity atoms. The asymptotic behavior of  $\sigma$  when  $T \rightarrow 0$  is indeed a more relevant criterium for specification:  $\sigma$  remains finite for a metal whereas  $\sigma \rightarrow 0$  for a semiconductor or an insulator. In amorphous metal, like Mg-Zn or Ca-Al, as there is no crystalline order to disturb, the conductivity does almost not depend on temperature. Comparisons with differently doped polymers show that their conductivities have different values, but all decrease with decreasing temperature. This decrease is however much slower than the one of crystalline semiconductors, like silicon for example, where the decrease of conductivity is essentially due to the freezing of conduction electrons. The reason for the conductivity decrease in polymers is due to the presence of localized states within the gap.

**Variable range hopping conductivity** Hopping is an abbreviation for "phonon-assisted quantum mechanical tunneling". In a disordered solid, there are some localized states<sup>3</sup> in the gap, randomly distributed in space

---

<sup>3</sup>It was first described by Anderson in 1958 in a paper called "The absence of diffusion in certain random lattices" and this localization got the name of Anderson's localization. Materials which have localized states at  $E_F$  are called "Fermi glasses" [25]

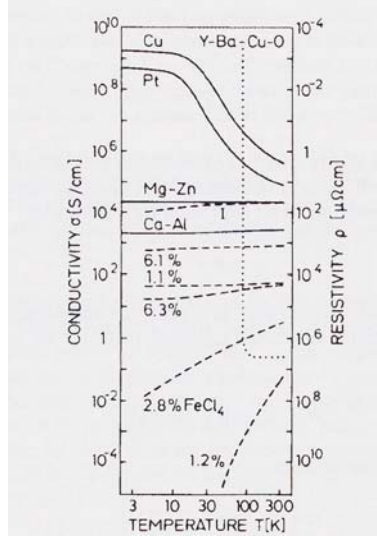


Figure 2.8: Comparison of conductivities for metals (solid) and various doped polymers (dashed lines) [24].

as well as in energy as shown in Fig. 2.9. If electrons are excited to delocalized states of energy  $E_C$ , then the conductivity is [24]

$$\sigma = \sigma_{E_C} \exp\left(-\frac{E_C - E_F}{kT}\right) \quad (2.5)$$

At room temperature, the available energy is too small for such an excitation, so the electrons have to hop (tunnel) from a state below the Fermi level to a near localized state above the Fermi level. The probability for such an event is proportional to the Boltzmann factor  $\exp(-W/kT)$ , where  $W$  is the energy difference between these two states. The probability depends also on the phonon spectrum and the overlap of the wavefunctions. Mott pointed out that the hopping distance  $R$  increases with decreasing temperature, thus the name variable range hopping, and came to the following dependence  $\ln\sigma \propto T^{-1/4}$ . It is in fact a particular case of the generalized form for conductivity given by [25]

$$\sigma = \sigma_0 \exp\left(-\left(\frac{T_0}{T}\right)^\gamma\right) \quad (2.6)$$

where  $\sigma_0$  is the conductivity in the limit  $T \rightarrow \infty$ ,  $T_0$  is a parameter that depends on the localization length and the electron density at Fermi energy,

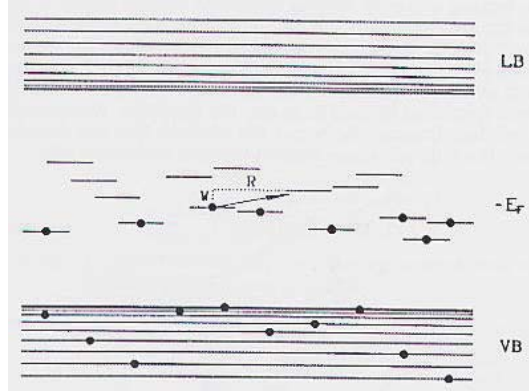


Figure 2.9: Electronic level scheme of a disordered solid that shows the hopping conductivity. CB is the conduction band, VB the valence band,  $E_F$  the Fermi energy,  $W$  the energy between states and  $R$  the local physical distance between states [24].

and  $\gamma$  depends on the dimensionality  $d$  of the hopping process and is given by

$$\gamma = \frac{1}{1 + d} \quad (2.7)$$

In practice, it is often difficult to clearly fit values for  $\gamma$  and thus to distinguish between one, two or three dimensional processes.

Those considerations are valid for a dc field. For an ac field, theories and experiments have shown that there is a dependence of the conductivity on frequency if the temperature is low and/or the frequency is high, as can be seen on Fig. 2.10.

### 2.3.3 Electric conductivity measurements on DNA

**First historical measurement** D. Eley and D. Spivey were among the first authors to measure the DNA electric conductivity. They reported in 1962 measurements of conductivity on DNA pellets in a pressure cell, where they contacted the pellets with platinum electrodes with a pressure of 70 kg/cm<sup>2</sup> and in vacuum [26]. They found conductivities following the law

$$\sigma = \sigma_0 \exp\left(-\frac{\Delta E}{2k_B T}\right) \quad (2.8)$$

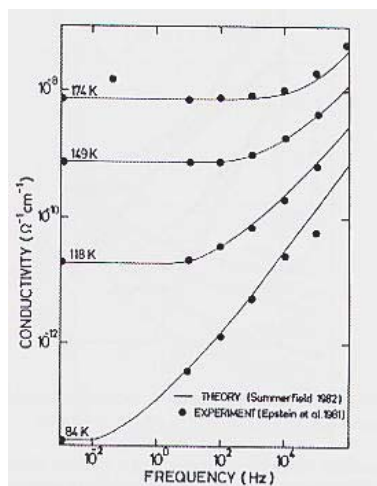


Figure 2.10: Conductivity as a function of frequency for undoped polyacetylene [24].

with a conductivity at 400 K in the order of  $10^{-12}(\Omega cm)^{-1}$  and energy gap  $\Delta E$  of 2.4 eV. They attributed this conductivity to the stacking of base pairs and the overlap of  $\pi$ -electrons<sup>4</sup>. They reported similar values for RNA. They said that little is known of the RNA structure to be able to comment this value, but nowadays one would expect a lower conductivity for RNA, as the overlap should be less good.

Using a similar method, Smart measured in 1973 an energy gap of 2.4 eV and a conductivity  $\sigma_0$  of  $6.3 \cdot 10^2(\Omega cm)^{-1}$  [27].

**Resonant cavity measurements** A technique using a resonant cavity has also been used to measure the intrinsic conductivity of DNA [28]. It uses a configuration that does not require contacts to be attached to the sample under study [29]. The material is placed in the high electric field region of a highly sensitive resonant cavity and the resulting change in the quality factor  $Q$  is measured.  $Q$  is inversely proportional to the energy loss  $W$ , and the loss due to the specimen is evaluated from the change (decrease) of  $Q$  upon the sample being inserted into the cavity. There is a relation between this loss  $W$  and the real part of the conductivity  $\sigma$ : for randomly oriented DNA

<sup>4</sup>In aromatic crystals, the conduction is parallel to the crystal plane whereas in DNA the conduction is perpendicular to the planes, thus the low measured conductivity (see Fig. 2.11)

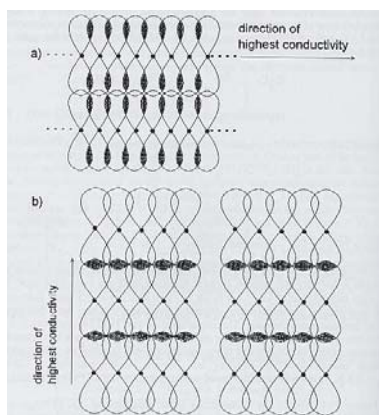


Figure 2.11: a) conduction parallel to the plane: two chains (ex. benzene) are shown  
 b) conduction perpendicular to the plane: two stacks (ex. DNA) are shown [24]

strands placed in a uniform electric field, the following relation is a good approximation

$$W = \frac{1}{3} V \sigma E_0^2 \quad (2.9)$$

where  $V$  is the volume,  $E_0$  the time averaged intensity of the applied ac field. The geometrical factor  $1/3$  is due to the random distribution of DNA segments. The formula could be verified with multiwall carbon nanotubes of known dc conductivity.

A resonant cavity encloses a volume whose dimensions are comparable to the desired wavelength and can support a series of modes each corresponding to a unique distribution of field. Most resonators are fabricated out of highly conducting materials so that the field is determined only by the boundary conditions at the inner surfaces. In a perfect cavity, the energy loss is zero and the quality factor infinite. In reality, the surface of the cavity has some finite impedance and the fields penetrate the walls as the effective shielding by the induced currents is reduced. Those losses give a finite  $Q$ . Measurements, typically as function of temperature, are done with the sample in the cavity and with the empty cavity. Typical frequency range is of order of  $10^{11}$  Hz with a cavity size of order of millimeter.

Dry DNA, DNA in buffer solution and buffer alone are measured. The results are shown in Fig. 2.12. The conductivity follows an exponential law

$$\sigma = \sigma_0 \exp(-\Delta/2kT), \quad (2.10)$$

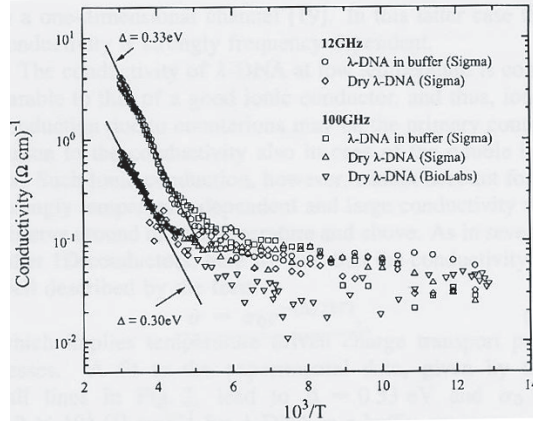


Figure 2.12: Conductivity of different  $\lambda$ -DNA at different frequencies as function of inverse temperature. The lines follow the law given by Eq. 2.10 [28].

showing essentially no dependence on the frequency. Data fits give the following values:

- $\Delta = 0.33 \text{ eV}$  and  $\sigma_0 = 1.2 \cdot 10^3 (\Omega\text{cm})^{-1}$  for DNA in a buffer environment
- $\Delta = 0.3 \text{ eV}$  and  $\sigma_0 = 1.9 \cdot 10^2 (\Omega\text{cm})^{-1}$  for dry DNA

It is pointed out that a simple semiconducting gap is unlikely, as the energy scale is significantly smaller than the main absorption band of the DNA helix in solution<sup>5</sup>. At room temperature, the conductivity  $\sigma$  is  $2.4 (\Omega\text{cm})^{-1}$  for DNA in buffer.

In Ref. [31], DNA is also measured in microwave cells (i.e without contact to it). The conductivity is deduced from the decrease of the microwave power reflected by the cell. The difference with Ref. [28] is that the charges are induced with pulses of 3 MeV electrons from a Van De Graaf accelerator, so the conductivity depends on the electron dose. Measurements are done at a fixed temperature (195 K) and for different degrees of DNA hydration. The conclusion is that the conductivity in B-DNA is due to mobile charge carriers within the outer mantle of the chain rather than within the base-pairs cores (notably due to the absence of anisotropy of conductivity for aligned fibers). There is however no explanation why these electrons do not become rapidly localized within the DNA core.

<sup>5</sup>Absorption measurements are typically done at wavelength of 260 and 280 nm (4.8 to 4.4 eV ) [30]

**Measurements with contacts on few molecules** The difficulty encountered with the measurement of the conductivity of one or few molecules is how to contact them. Several approaches are described in this section.

Trials have been done with scanning tunneling microscope (STM), as shown in Ref. [32]. Due to the high conductivity of the adsorbed water to the surface, the authors can image DNA on an insulating surface like mica. For this purpose, they evaporate a Pt-C ring shaped electrode over mica, and then image in the middle of the ring. An interesting point is that, in the middle of the loop formed by plasmid DNA, the substrate appears lower. The reason is that the tunneling voltage is higher (i.e. the voltage needed to get the set point of tunneling current) due to the fact that DNA acts as a lateral conductivity barrier. No specific measurement on the longitudinal conductivity of DNA are done in this experiment.

Some other groups, like the one of Kawai (Ref. [33] and references therein), have nice images of DNA with UHV STM, but on copper surfaces, thus without the possibility to measure the electric conductivity of the DNA.

An instrument whose mechanisms are close to transmission electron microscope (TEM) but with a completely different energy range is the so-called LEEPS microscope (Low Energy Electron Point Source) [34]. Thanks to this instrument, H.-W. Fink could make in 1998 an experiment that really launched the electrical measurements on single DNA molecule, since it is possible with it to visualize the DNA and to measure its conductance simultaneously [35]. Further explanation of the mechanisms of the LEEPS microscope and this experiment are given in Appendix B. The quite unexpected result of the experiment is the low resistance of the device (contacting tip, rope of few DNA and contacting grid, measured in high vacuum at room temperature): up to 2.5 M $\Omega$  for a 600 nm long DNA rope.

An alternative to STM is the use of AFM (atomic force microscope, also called SFM for scanning force microscope) with a metallic coated tip. The group of de Pablo [36] randomly deposited randomly  $\lambda$ -DNA on a mica surface, evaporated two gold electrodes separated by a thin wire acting as a mask (see Fig. 2.13). They can either apply a voltage through the two electrodes or through one electrode and the metal tip. With voltages up to 10 V and a resolution current below 1 pA, they estimate a minimum value for the conductivity of  $10^{-4}(\Omega cm)^{-1}$  in the case depicted in Fig. 2.13, and  $10^{-6}(\Omega cm)^{-1}$  when around one thousand molecules span the two electrodes distant of 15  $\mu m$ .

With almost the same configuration but in vacuum, the group of Kawai

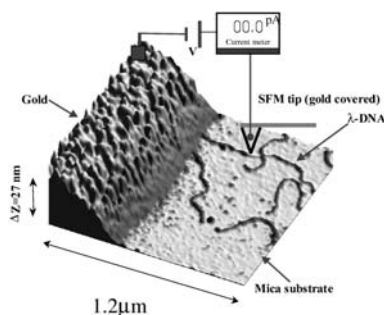


Figure 2.13: Three-dimensional AFM image showing DNA molecules in contact with gold electrodes and a scheme of the conductivity measurement [36].

[37] measured the conductivity of networks of poly(dG)-poly(dC) and poly(dA)-poly(dT) and obtain values of  $1 (\Omega cm)^{-1}$  and  $0.1 (\Omega cm)^{-1}$  respectively for a distance of 50 nm. The conductance decreases exponentially with increasing distance: a factor 10 for roughly 75 nm.

The last possibility is to have two electrodes made beforehand, and then bridge DNA over them to make the electrical contact.

The group of Yoo [38] measured several features of poly(dG)-poly(dC) and poly(dA)-poly(dT) sequences: current versus voltage for various gate voltages and temperatures. They used Au/Ti electrodes designed with lithography and angle evaporation: the distance between them in 20 nm. They observe almost no effect of water on the conductivity. They have essentially the same temperature behavior as the one observed by Grüner [28]. From gate measurements, they conclude that poly(dA)-poly(dT) behaves as a n-type semiconductor with a conductivity of  $40 (\Omega cm)^{-1}$  at zero gate, and poly(dG)-poly(dC) as a p-type semiconductor, as schematically depicted in Fig. 2.14.

Also with two pre-designed electrodes, Porath et al. [39] made measurements on poly(G)-poly(C) (10 nm length) and get large-bandgap semiconducting behavior in air and in vacuum down to cryogenic temperature, with current around 1 nA for 4 V. In a more recent experiment [40] but with larger distances (40 to 500 nm), the same group have reported a minimum device resistance value of  $10 T\Omega$ , with a resolution current below 1 pA for bias voltage up to 10 V. The device consists of one DNA molecule on  $SiO_2$  or mica surface and different electrodes materials (platinum or gold). Different types of DNA have also been tested: poly(G)-poly(C) or DNA modified with sulfur group to enhance the bonding with the electrodes.

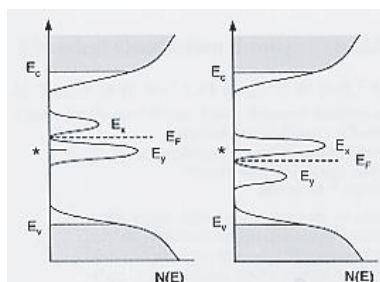


*Figure 2.14:* Schematic representation of the density of states  $N(E)$  for poly(dA)-poly(dT) (left) and poly(dA)-poly(dT) (right).  $E_c$  and  $E_v$  represent the conduction and valence bands, whereas  $E_x$  and  $E_y$  the localized states. The Fermi level  $E_f$  lies above the middle of the band gap (the asterisk) for poly(dA)-poly(dT) and below for poly(dG)-poly(dC) [38].

A very different behavior has been observed in the experiment of Kasumov et al. [41] who could measure very low resistances at room temperature (less than  $100 \text{ k}\Omega$  per DNA molecule over  $0.5 \text{ }\mu\text{m}$ ) and a weak dependence as function of temperature. Below the superconducting transition temperature of the contacts (1 K, Re/C electrodes), they even observed proximity-induced superconductivity. It implies that the molecules are good conductors, that their phase coherence length is on the order of the length of the molecule, and that they form a low-resistance contact with the superconducting electrodes.



# Chapter 3

## DNA as fiber

### 3.1 Introduction

As mentioned in Chap.2, different behaviors are expected from measurements on bulk or on mesoscopic size sample. For the case of inhomogeneous material like polymer or DNA film, conductance measurements on single molecules (or rope of several strands) or on large amount of molecules either crystalized or entangled in a random network will certainly give different results. One of the main reasons is that with a large amount of molecules, one measures simultaneously properties of the molecule and of the network, like its connectivity typically.

The method of measuring a film is often used in the field of conductive polymers characterization (see Ref. [42] and references therein). It is also found that if some arrangement can be done inside the film, the conductance is increased due to the better alignment of the molecules (in polypyrrole for example [43]). The same behavior can be observed with films made out of DNA molecules [44, 45]. The obtained film can be stretched in one direction by a factor 2 to 3, leading to an increase of conductance in the stretched direction by a factor of  $10^2$  to  $10^4$ . Note that in the preparation of the film, the authors exchange the sodium counter ions of the DNA with cationic amphiphiles molecules: the film is thus water-insoluble. Calf-thymus DNA films measured in a microwave cells also show the influence of the film internal orientation [31]. In an electrochemical study, the rate of electrochemical reactions can be related to the diffusivity of electrons or hole in the sample under experiment and different results are obtained for different DNA [46]:

- for disordered ds-calf thymus, no rate can be observed
- for ss-12 oligo, no rate can be observed
- for ds-12 oligo, the rate is  $1.5 \pm 0.2 \text{ s}^{-1}$
- for ds-12 oligo with two mismatched base pairs, the rate is  $0.6 \pm 0.2 \text{ s}^{-1}$ .<sup>1</sup>

One of the conclusions, besides other considerations about the influence of base mismatch, is that alignment is required to have charge migration.

In this chapter I present the experiments done in our group with DNA fibers, i.e. how we prepare them, contact them and measure the conductivities as a function of several external parameters. We decide to prepare macroscopic fibers of DNA rather than films, as the preparation of them requires more chemical skills. As the preparation procedure of fiber will show, it is also a way to have DNA at least partially aligned.

## 3.2 Experimental preparation

A DNA fiber is prepared as follows. Calf-thymus DNA comes out as a network of dried, white entangled chains of DNA that look a bit like wool. One takes out several small pieces of it and mix them with few microliter of a buffer solution in order to get a sticky paste<sup>2</sup>. A drop is picked up with a tweezer, and by opening and closing the tweezer several times, a fiber can form between the two ends of the tweezer, as shown in Fig. 3.1. This is achieved once the orientation of the DNA strands and the water concentration of the solution, slowly decreasing from original one by evaporation, are appropriate. The obtained fiber has typical dimensions of 4 to 5 mm in length and 10 to 100  $\mu\text{m}$  in diameter. It is dried overnight either in air at room temperature or at 5°C for a slower drying.

The fiber is so light that it cannot be laid down over a surface without a minimum pressure on it. We evaporate first two large gold pads on a ceramic plate (10x10x1 mm<sup>3</sup>) of high resistivity ( $\rho > 10^{16} \Omega\text{cm}$ ). The gap between

---

<sup>1</sup>They use the calf-thymus DNA as it is and monolayers of one-dimensionally aligned 12-base pair single or double stranded DNA chemically linked to the electrodes. If only the chemical linkers are present, the rate is around  $5 \pm 1 \text{ s}^{-1}$

<sup>2</sup>See Appendix C for details

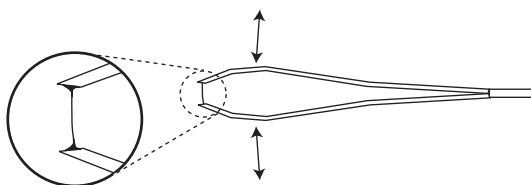


*Figure 3.1:* Preparing a DNA fiber with a tweezer. After several openings and closings, a fiber forms at the end. Once dried, it can be manipulated safely.

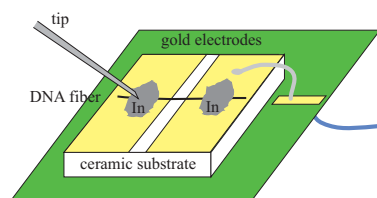


*Figure 3.2:* Scheme of the ways to contact a DNA fiber. On the left is shown a contact with the tip that can contact either the indium or the gold. On the right is shown a contact with a copper wire to an electronic contacting plate.

the two pads is roughly 2 mm, and the contacts with the fiber are achieved with small indium pieces pressed over it, as shown in Fig. 3.2. The indium has the advantage that it is a soft material, thus ensuring a better electrical contact with the DNA fiber (high surface contact) without destroying it. It is also possible to contact the gold pads, either with standard prober tips, or with a small copper connected with an electronic contacting plate that is then portable to a vacuum chamber for example. The contact to the gold pads has the advantage that one does not touch the indium pads anymore and hence avoid to take them off.

Experiments are also done with a state-of-the-art prober (NAGASE BCT-21 MBC) with vacuum chamber, gas inlets and temperature control. With this prober, the contacts to the indium pads are achieved with two tips controlled from outside the chamber by micrometric screws, with the advantage that contacts can be always verified also in vacuum. A picture and scheme of the prober is shown in Fig. 3.3, and a picture of a contacted fiber in Fig. 3.4.

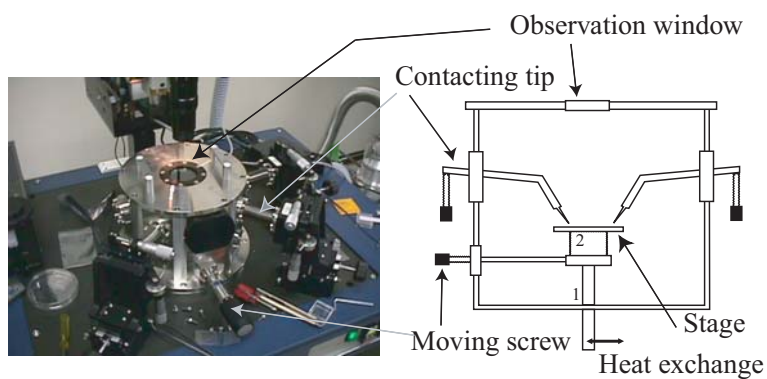


*Figure 3.3:* Picture and scheme of the prober used to measure the fiber conductivity. Thermocouples measure the temperature at point 1 and 2. The tips are controlled by micrometric screws. A CCD camera mounted on top of the observation window helps for a better visual control (not seen on picture)

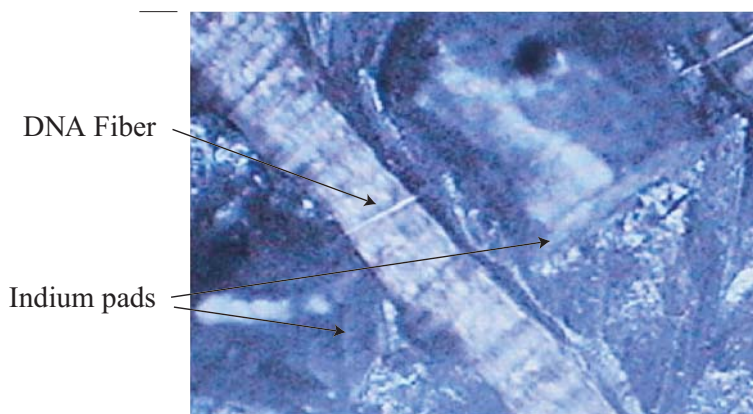


*Figure 3.4:* CCD picture of a DNA fiber contacted with indium pads and mounted in the NAGASE prober (shown in Fig. 3.3.) The distance between the two pads is around 1 mm.

### 3.3 Conductivity measurements

Most of the measurements are carried with a lock-in amplifier (Stanford Research SR830 or NF Electronics Instruments, LI 5640) that measures the current response (amplitude and phase shift) to an excitation voltage  $U$  at frequency  $f$ . The ability of the lock-in to measure small ac-signals makes it particularly useful for conductivity measurements on DNA, where high resistances are expected<sup>3</sup>.

When measuring small ac current, one must take care of artefact, especially inductive or capacitive couplings. Control experiments and characterization of the circuit without the sample under test are used as reference.

A ceramic plate with indium pads and contacted with tips is measured as reference (Fig. 3.5). The uncertainty of the current is around 1 pA for this set-up, so the current values below 1 pA are not relevant. Above this limit, the curves show almost perfect linear increase of current as a function of frequency and a phase shift of 90 °, which is the behavior of a capacitor. With the relations

$$I = U/Z \text{ and } Z = 1/\omega C \quad (3.1)$$

where  $Z$  is the impedance,  $U$  the applied voltage,  $\omega = 2\pi f$  (frequency  $f$ ) and  $C$  is the capacitance, the capacitance can be calculated for each curve:

$$C_a = \frac{7.84 \cdot 10^{-11} \text{A}}{400 \text{Hz} \cdot 2\pi \cdot 0.1 \text{V}} = 310 \text{ fF} \quad (3.2)$$

$$C_b = \frac{3.9 \cdot 10^{-9} \text{A}}{400 \text{Hz} \cdot 2\pi \cdot 5 \text{V}} = 310 \text{ fF} \quad (3.3)$$

As expected from the identic slopes, they are the same.

When a fiber is contacted, the measured current is the sum of the current going through the fiber with resistance  $R$  and the displacement current going through the capacitance  $C$ . If the resistance  $R$  is smaller than  $1/\omega C$ , a pure resistive behavior will be observed: the current will be independent of frequency and the phase difference will be small (ideally zero).

A typical measurement is shown in Fig. 3.6, where a fiber is first measured in air, then in vacuum, and then in air again. On curves (a) and (b), the

---

<sup>3</sup>Measurements with a dc excitation (Keithley 6430) give basically the same resistance values but without the advantages of the lock-in.

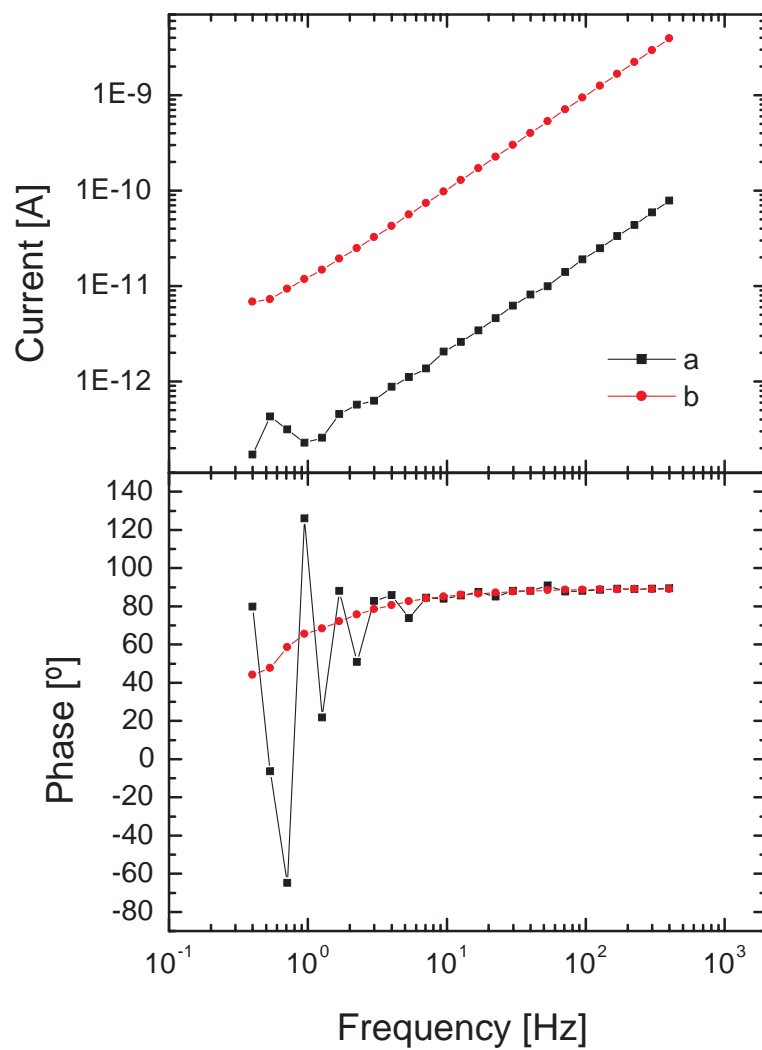


Figure 3.5: Measurement of ceramic plate without fiber: a)  $U = 0.1\text{V}$ , b)  $U = 5\text{ V}$ .

fiber shows a resistive behavior below 10 Hz. In a frequency interval between 10 Hz and 200 Hz, the current going through the fiber and the displacement current are of similar magnitude. Above 200 Hz, the behavior is mainly capacitive. With  $I = 5.5 \cdot 10^{-7}$  A,  $f = 16$  kHz and  $U = 5$  V, the capacitance is  $C = 1$  nF. The curve (c) leads to the same value for  $C$  ( $I = 4.1 \cdot 10^{-10}$  A,  $f = 13.9$  Hz). The resistance  $R$  is given by the plateau value of the current at low frequency divided by the voltage: 1 G $\Omega$  for curves (a) and (b) and 5 G $\Omega$  for curve (c). In vacuum, a minimal resistance for the fiber can be estimated, in the order of 1 T $\Omega$  ( $I < 5 \cdot 10^{12}$  A).

Measurements with the NAGASE prober show essentially the same behavior. An example is shown in Fig. 3.7. The way of contacting, slightly different than with the other set-up, leads to capacity values that are smaller, probably due to a better isolation of the tips, as only their very end is naked. Those capacity values vary also proportionally more from one sample to the other, as the indium pads have to be changed more often. They never exceed however a value of 1 pF.

The measurement of the current as a function of the voltage shows a linear behavior, and the resistance of the fiber can be deduced when measured at a frequency where the capacity has no influence. Measurements with the same fibers as in Fig. 3.7 are shown in Fig. 3.8. The resistance of the quartz plate  $R_q$  and the resistance of the fiber  $R$  are in parallel, so  $R = R_{mes}R_q/(R_q - R_{mes})$ , where  $R_{mes}$  is the resistance given by the applied voltage divided by the measured current.

Different experiments with different fibers show a resistance range from 0.1 to 500 G $\Omega$ . To see the respective influence of size (length  $l$ , diameter  $d$ ) and other parameters, the conductivity  $\sigma$  is calculated:  $\sigma = 4R/(\pi d^2)$ . The relative uncertainty  $dl/l$  is estimated as 20% and the relative uncertainty  $dd/d$  up to 20%, depending on the fiber shape. The values for  $\sigma$  range from  $1 \cdot 10^{-8}$  to  $8 \cdot 10^{-5}(\Omega \text{ cm})^{-1}$  with a relative uncertainty of 50%. Although the uncertainties on the fiber dimension are quite large, they do not explain the large range of measured conductivities. Therefore different external parameters are investigated, as presented in the next section.

### 3.3.1 Influence of external parameters

We measured the influence of several parameters on the DNA conductivity. These are the gas and humidity environment of the fiber and the solution

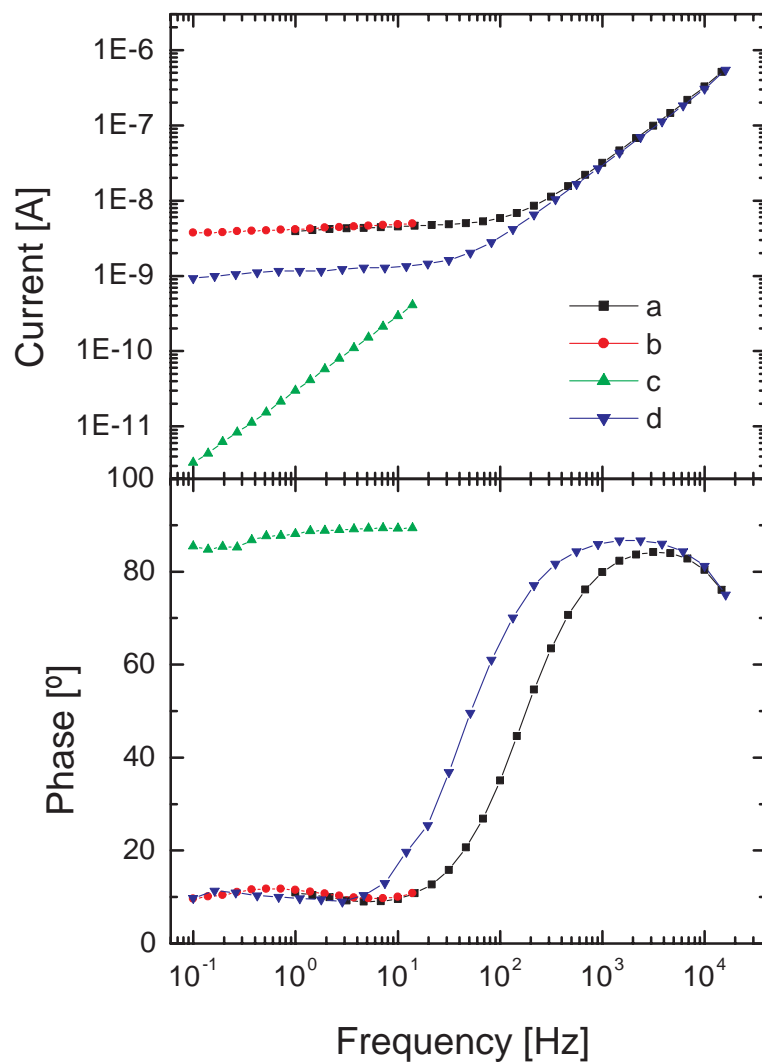


Figure 3.6: Measurement of a DNA fiber ( $l \approx 1.5$  mm, diameter  $d \approx 33 \mu\text{m}$ ) at  $U = 5$  V. (a) and (b) are measured in the air, (c) in vacuum and (d) in air again. (b) and (c) are measured with higher sensitivity on the lock-in, hence the smaller scanned range [47]

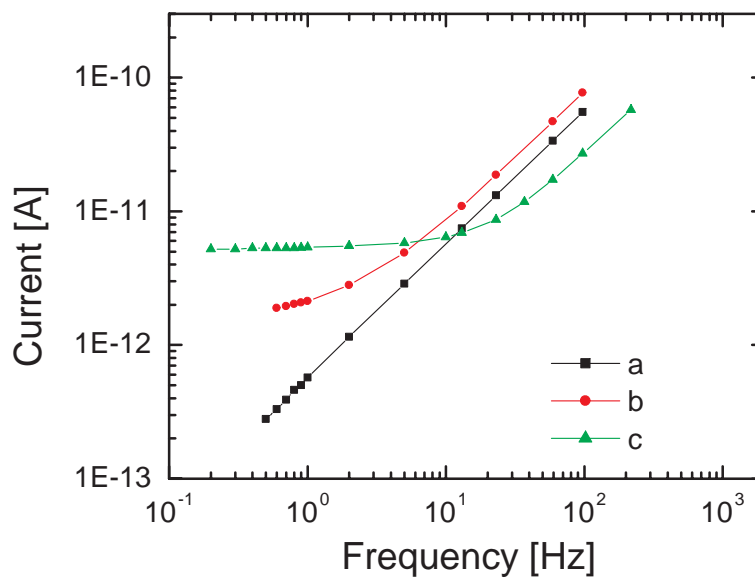


Figure 3.7: Current/frequency graphs measured with prober shown in Fig. 3.3. Voltage is 1 V. ( $l \approx 1$  mm, diameter  $d \approx 70 \mu\text{m}$ )

(a) Sample with indium contacts but without DNA.

(b) Same contacts as in (a), but with DNA fiber.

(c) Other fiber and other contacts.

$C$  is estimated for curves (a) and (b) as 50 fF and for curve (c) as 130 fF.  $R$  is estimated for curve (b) as 500 G $\Omega$  and for curve (c) as 200 G $\Omega$ .

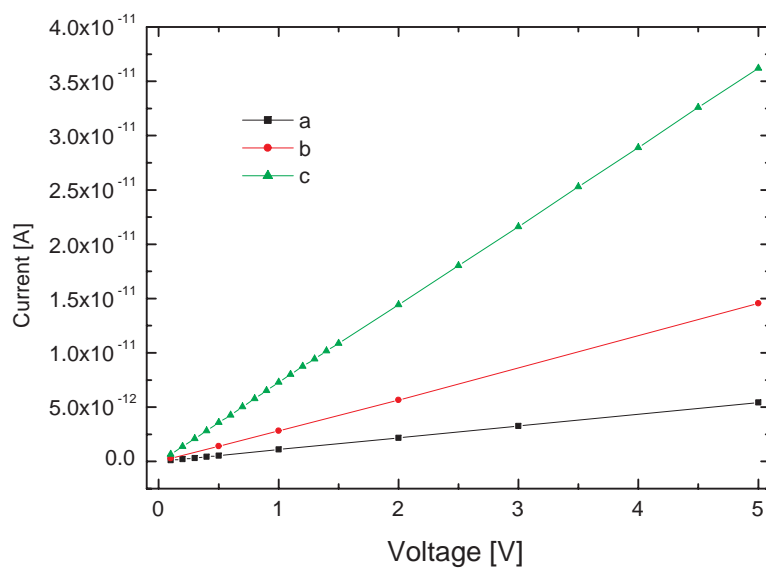


*Figure 3.8:* Current/voltage graphs measured on the same fibers as in Fig. 3.7. The frequency is 1.9 Hz.

The resistance of the quartz plate  $R_q$  ( $900 \text{ G}\Omega$ ) and the resistance of the fiber  $R$  are in parallel. The resistances of the fibers are the same as when estimated from current/frequency curves, i.e.  $500 \text{ G}\Omega$  for curve (b) and  $200 \text{ G}\Omega$  for curve (c).

used to prepare the fiber and the temperature at which the fiber is measured. It is known from the polymer science that the electrical conductivity can be strongly influenced depending on the level of doping [48]. Doping is typically done by oxidation or reduction, hence the use of oxygen. It is also interesting to test solutions with different ions, as monovalent or divalent ions are known for being able to change the DNA alignment of bases or the DNA stability [49].

To check the influence of gases, measurements are done in a chamber that can be evacuated and then filled with the desired gas. Already at one tenth of an atmosphere pressure, the device exhibits a purely capacitive behavior, with the same properties as the set-up without any fiber: there is no measurable current. If the chamber is refilled with air, the fiber recovers its original value (at least 50%) with a speed roughly inversely proportional to the time it has been in vacuum. If the chamber is filled with nitrogen, the behavior is the same as in vacuum: no current. Humidity, present in air, but absent in vacuum or nitrogen, is then the key parameter to have a measurable current through the fiber. If humidity is artificially increased inside the chamber, the conductivity immediately increases (up to factor 2). It is not possible to measure in saturated humidity as the fiber is then dissolved.

The ability of oxygen to increase the fiber conductivity is also tested. The behavior remains the same as in vacuum: no measurable current. The fact that no effect is observed can be due to the kind of DNA measured. Following Ref. [38], AT sequences are n-type semiconductor and GC are p-type, as G is easily oxidized, so the influence of an oxidizing agent might have little influence on a random sequence DNA, as is  $\lambda$ -DNA. It is also possible that the molecular oxygen is not a sufficiently strong oxidizing agent for our kind of fiber.

The influence of the ions in the solution used to prepare the fiber is also investigated. A very systematic study can unfortunately not be done because the solution has a strong influence on the stability of the fiber, so some fibers are difficult or impossible to form. The idea is typically to test monovalent and divalent ions, i.e. water solutions with NaCl or MgCl<sub>2</sub>. Fibers are prepared with a solution of 1 M NaCl, but they cannot form with a solution of 1 M MgCl<sub>2</sub>. Fibers are then prepared in a solution containing the two

	$\sigma$ of solution $[(\Omega\text{cm})^{-1}]$	$\sigma$ of fiber $[(\Omega\text{cm})^{-1}]$
DI water	$5 \cdot 10^{-8}$ (a)	$1 \cdot 10^{-8}$ to $8 \cdot 10^{-5}$ (d)
1 M NaCl	$7 \cdot 10^{-3}$ (b)	$6 \cdot 10^{-5}$ (e)
0.5 M NaCl/0.5 M MgCl <sub>2</sub>	$1 \cdot 10^{-2}$ (c)	$1.5 \cdot 10^{-3}$ (e)

*Table 3.1:* Conductivities of the solutions and of the DNA fibers prepared with them.

a) conductivity set-point of the DI water (18 M $\Omega\text{cm}$ )

b) given by Ref. [50])

c) calculated from conductivities for NaCl and MgCl<sub>2</sub> according to Ref. [50]

d) values for  $\sim 15$  fibers,  $\sim 40$  measurements. Relative uncertainty is 50%

e) values for 1-2 fibers, 4-5 measurements. Relative uncertainty is 100%

Fibers measured in vacuum have a resistance in the T $\Omega$  range or bigger, i.e. conductivities of  $10^{-9}$  ( $\Omega\text{cm}$ )<sup>-1</sup> or smaller, independently of the solution.

salts: 0.5 M NaCl/0.5 M MgCl<sub>2</sub>. Those fibers are less 'wire-like' than the one in deionized water, in the sense that their section is not uniform: the relative uncertainty of the diameter is around 50%. The conductivity have then a relative uncertainty around 100%.

The measurements are shown in Fig. 3.9. The conductivities are estimated as  $\sigma_{Na} \approx 6 \cdot 10^{-5}(\Omega\text{cm})^{-1}$  for a fiber prepared with a solution 1 M NaCl and as  $\sigma_{NaMg} \approx 1.5 \cdot 10^{-3}(\Omega\text{cm})^{-1}$  for for a fiber prepared with a solution of 0.5 M NaCl/0.5 M MgCl<sub>2</sub> .

The table 3.1 summarizes the measured conductivities of fibers as well as the conductivities of the solution used to prepare them.

The fact that the DNA fibers prepared with NaCl solutions have a comparable conductivity with some of the fibers prepared only with deionized water is not surprising, as the calf thymus indeed comes with sodium ions.

The fact that DNA fibers prepared in salty solutions have a smaller conductivity than the solution itself is not surprising: the mobility of the ions is much smaller in the fibers than in solutions. On the other side, they have a larger conductivity than the fibers prepared with deionized water. The following simple model can qualitatively explain it.

Fibers can be considered as an ensemble of DNA strands with tightly bound water molecules, tightly bound ions and a water mantle around them. The thickness of this water layer depends certainly on the humidity level. A proportion of the ions are tightly bound to the DNA, but the other are more mobile, thus the more humid the environment, the larger the available volume for them. Those ions are believed to be responsible for the measured

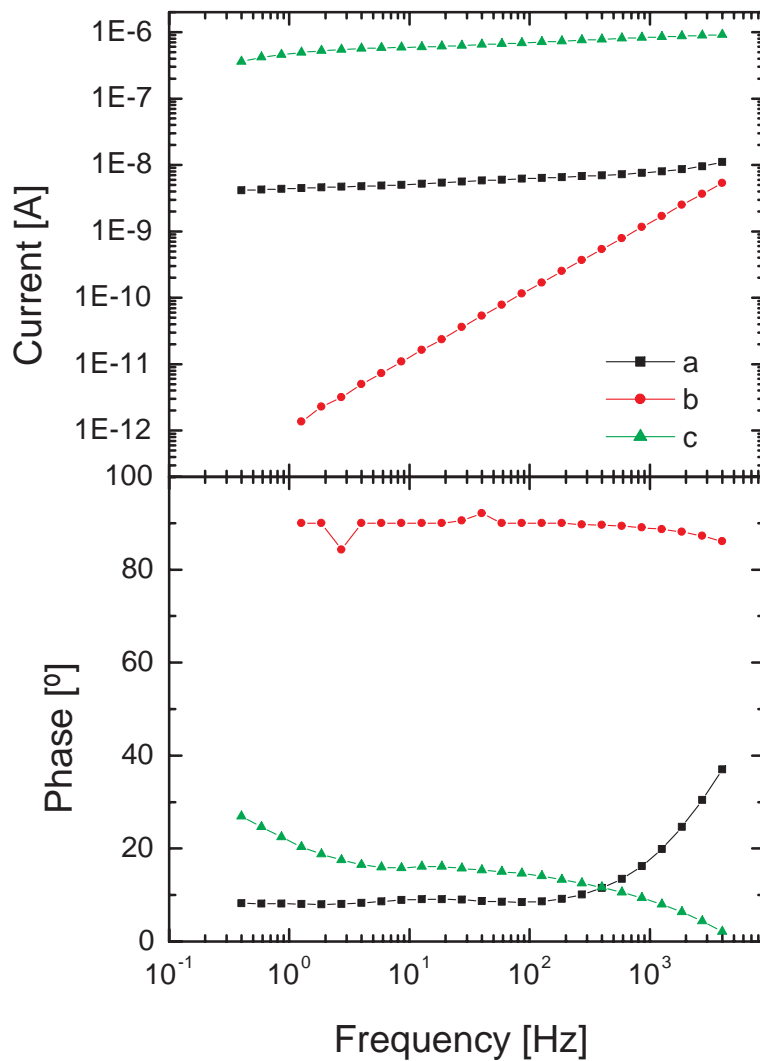


Figure 3.9: Current/frequency measurements at voltage  $U = 0.2$  V.

(a) and (b): fiber prepared in a 1 M NaCl solution (diameter  $\approx 120 \mu\text{m}$ , length 0.7 mm) and (c) 0.5 M NaCl and 0.5 M MgCl<sub>2</sub> (diameter  $\approx 50 \mu\text{m}$ , length 0.5 mm).

(a) and (c) are measured in room conditions, (b) in vacuum.

current.

Another fact tends to confirm this model: a larger conductivity is observed for a fiber surrounded by magnesium ions than for one surrounded only by sodium ions. Magnesium ions have a shorter screening length than sodium ions<sup>4</sup>, so the ions in the water mantle are more mobile when some magnesium ions are tightly bound to the DNA. The fiber is then more conductive.

The influence of the temperature can only be tested in the NAGASE prober, which stage is temperature controlled via a heat exchange on its bottom: a thermocouple measures the temperature close to the stage (see Fig. 3.3). It is only possible to cool the sample, not to warm it.

Measurement as a function of the temperature fails at room conditions, because the humidity variations due to the change of temperature mask any temperature contribution. In vacuum, no current is measured down to a temperature of 183 K.

### 3.4 Conclusions

The most influent parameter in our experiments is clearly the humidity level. It is demonstrated by the fact that no conductivity is observed either in vacuum, nor in a nitrogen environment. The likelihood that the high resistance measured in vacuum is only due to high contact resistances between the DNA strands forming the network is small: a rough estimation of the number of contacts inside a fiber (1 mm length, 100  $\mu\text{m}$  diameter) of aligned rods (10  $\mu\text{m}$  length, 2 nm diameter) gives  $n_l = 10^{-3}/10^{-5} = 100$  contacts to put in series and  $n_s = (50^{-6})^2/(10^{-9})^2 = 2.5 \cdot 10^9$  contacts in parallel. With a resistance value  $R$  of 1 G $\Omega$  for each, it gives a resistance value of  $R_{tot} = 2Rn_l/n_s \approx 100 \Omega$ , i.e. negligible compared to the measured resistance. Because there are so many strands in parallel in a fiber and the conductivity of fibers is still low, the conclusion is that the DNA itself must be a very poor conductor in these conditions. We will explore in Chap.4 what happens when one tries to access to the conduction of devices with individual molecules.

---

<sup>4</sup>In solution, the electrostatic potential due to a charge at a distance  $d$  is proportional to  $\exp -\kappa d$ .  $1/\kappa$  is called the Debye-Hückel screening length and is in inverse proportion to the charge of the ions [30]. It ranges from  $\text{Å}$  to nm, depending on the ions concentration

# Chapter 4

## DNA as single molecule

The measurement of single molecule properties raises several challenges. One of them is how to manipulate and position the molecule where it needs to be measured without damaging it so much that the measurement gets meaningless. Another one is the control technique, i.e. checking what is really spanning the electrodes, that must also be of as little influence as possible. If it is not possible, it has to be done after the measurement.

In this chapter two different techniques used to place DNA between contact electrodes are presented. First, for each of them brief explanations about the involved mechanisms are given, and then descriptions and results of our experiments. The third section presents an electrical characterization of single DNA molecules, notably as function of the positioning technique.

### 4.1 Hydrodynamic stretching

#### 4.1.1 Mechanisms

In an aqueous solution, the DNA molecule adopts a conformation determined by two opposing phenomena. On the one side its rigidity, due essentially to the stacking of the bases, straightens it, and on the other side the thermal forces bend it randomly. This interplay leads to a persistence length  $P$ , which is the length scale on which the directionality is maintained [51]:

$$P = \frac{\kappa}{k_B T} \tag{4.1}$$

where  $\kappa$  is the torsional elastic constant and  $T$  the absolute temperature. For DNA in a moderate salt concentration (10mM NaCl),  $\kappa = 3 \cdot 10^{-28} \text{Jm}$  [52], so  $P$  is around 50 nm.

When one zooms into scales shorter than  $P$ , the molecule appears straight, but looked at from a further distance, the molecule bends this way and that, and appears to be randomly coiled. This description is called worm-like chain (WLC): the DNA is treated as a uniform elastic rod. Viewed under a microscope, the molecule looks like a random coil with a mean square distance  $\langle R^2 \rangle$  between its two ends given by [51]

$$\langle R^2 \rangle = 2PL \quad (4.2)$$

where  $L$  is the contour length of the molecule. For lambda-DNA, ( $L = 16.4 \mu\text{m}$ )  $R = 1.3 \mu\text{m}$ .

Another model to describe a polymer in solution is the freely jointed chain (FJC), where the polymer is represented as a chain of  $N$  rigid rods of length  $b$  connected by revolving pivots. A correspondence between the equilibrium configurations of the WLC and FJC is ensured by the choice  $b = 2P$  [51].

Both models describe what happens when a force is exerted on the molecule to unfold it. A force is necessary because the number of molecular configurations consistent with a given end to end distance decreases if this distance increases. The models can give a quite good relation between force and proportional extension as long as this extension remains small, i.e. the distance is shorter than the contour length. It corresponds to the part (a) of the curve shown in Fig. 4.1. If the chain has to be extended over its contour length, the force required depends then on Young's modulus of the DNA (part b), where the Hooke's law is valid:

$$F/A = E\Delta l/l \quad (4.3)$$

where  $F$  is the force,  $A$  the cross section,  $E$  the Young's modulus ( $\approx 10^8 \text{Pa}$  [54]),  $\Delta l$  the extension and  $l$  the length.

For larger extension (domain c and d), both models (FJC and WLC) fail because they do not take into account the deformation of DNA, that indeed undergoes a phase change from B-DNA to S-DNA [53].

Most of the experiments studying the mechanical properties of a DNA molecule in solution use optical tweezers to handle it. In such experiments, a DNA molecule is attached by one end to a latex bead, for example, and the other side can be anchored to a surface or to a pipette via another bead.

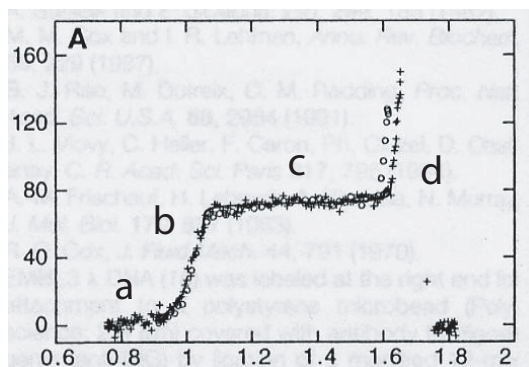


*Figure 4.1:* Force (pN, left axis) versus relative extension for a DNA molecule. Different regimes can be distinguished: the force is exerted against entropy in (a) and again Hooke's energy in (b). The regime in (c) is called inextensible worm-like chain: there is a structural change from B-DNA to S-DNA (S for stretched) [53]. A further extension (d) reveals a larger value for the Young modulus.

By trapping the bead at the focus point of an optical objective, usually with laser light, one can manipulate the molecule (see for example Ref. [55–57]). Another method is to anchor DNA molecules on the surface and to stretch them by a receding meniscus [58]. Physical quantities like forces or elastic modulus can be deduced from fluorescence microscope images. An estimation of the force acting on a DNA at the meniscus is given by  $F = \gamma\pi D \approx 400$  pN, where  $\gamma = 7 \cdot 10^{-2}$  N/m is the surface tension for the air water interface and  $D = 2.2$  nm is the diameter of the DNA. This force is large enough to stretch DNA. This estimation does not take into account the contact surface tension, but in reality one expects different forces for surfaces with different contact surface tension, as hydrophilic or hydrophobic surfaces for example.

### 4.1.2 Experiments

The basic of hydrodynamic stretching is applied to ultimately stretch DNA across the electrodes. Experiments are run first on surfaces without electrodes to test the influence of different parameters. An example of a simple experiment is shown in Fig. 4.2: on a chemically modified silicon oxide surface<sup>1</sup>, a drop of stained DNA was placed. After 10 min., the drop was blown

<sup>1</sup>10 min in a bath of 1/100 APTS/toluene (water free), then rinsed in toluene, isopropanol, and 10 min. in an oven (100°C) to evaporate the toluene

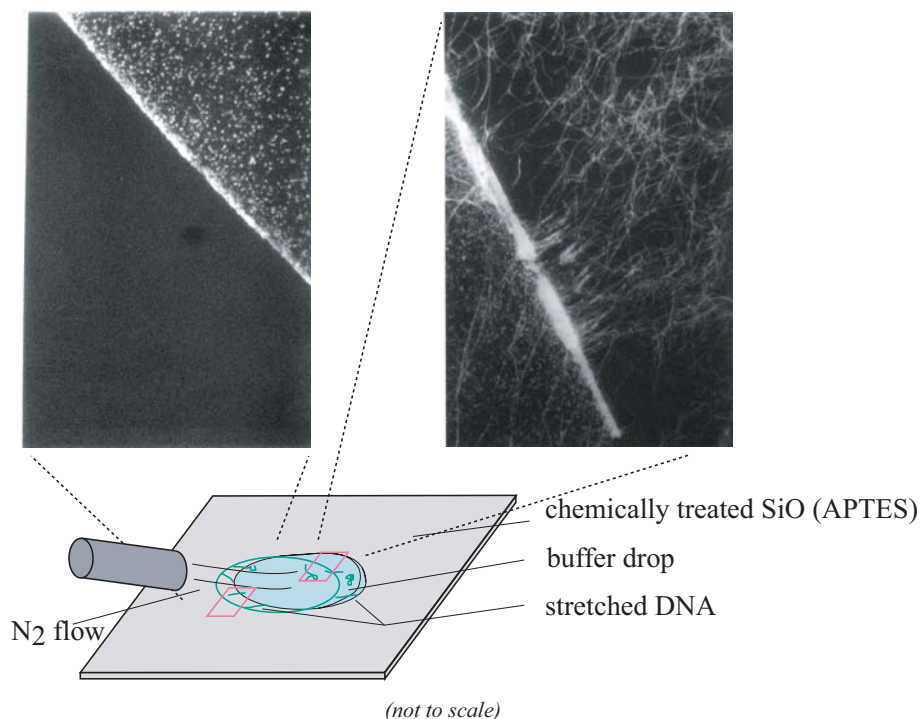


*Figure 4.2:* A schematic of simple DNA stretching. The two squares show roughly where the pictures are taken. Their size is  $135/85 \mu\text{m}$ . There is an accumulation of DNA at the border of the drop, and a lot of randomly stretched DNA on the right part of the drop. As expected, there are no DNA on the left part of the drop. The speed of stretching is on the order of mm/sec. Inside the drop, lot of unstretched DNA, that appear as dots, can be seen.

away with a flow of  $\text{N}_2$ . The sample was then rinsed gently in deionized water and imaged with a fluorescence microscope (Appendix B and C give the observation technique details and the staining recipes). The DNA used is  $\lambda$ -DNA, where the term lambda means that the molecules are extracted from a  $\lambda$ -bacteriophage and does not refer to a structural conformation like B-DNA or S-DNA (Appendix C give information on the molecule).

To get a more reproducible flow and hence a better control of the stretching of DNA, the following apparatus was prepared (see Fig. 4.3). A cylinder is filled with a DNA buffer solution into which the sample is dipped. Then the solution is evacuated with a microliter pump: the movement of the receding meniscus stretches the DNA. The sample is gently rinsed with deionized water before the observation with the fluorescence microscope.

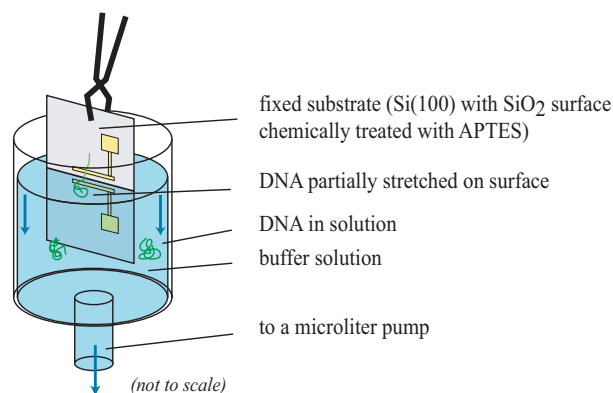


*Figure 4.3:* The hydrodynamic stretching cylinder: the receding meniscus stretches the DNA perpendicularly to the meniscus line.

We tested several parameters, and in particular the surface treatment of the silicon substrate, the pH of the solution, the DNA concentration, the duration and the speed of the stretching. Here is a brief review of their relative influence.

The speed of pumping is given in volume/min: with a flow rate of 1 ml/min, the 1 ml cylinder is evacuated in one minute, with a meniscus speed of 1 cm/min (i.e. 150  $\mu\text{m/s}$ , roughly ten times slower than with nitrogen flow). This value is larger than some literature values (for example in Ref. [57], the flow is 20  $\mu\text{m/s}$  to have full elongation, or in Ref. [58] the meniscus speed is about 5  $\mu\text{m/s}$ ), but a lower one leads to poor stretching. In fact, the time the sample is dipped in solution is a more critical parameter than the speed of stretching. If it is too long, too many DNA come by diffusion close to the surface and bind in a coiled form, which appear as dots on the fluorescent picture as observed inside the drop (Fig. 4.2). The high speed avoids this phenomenon.

The DNA concentration is also quite easy to adjust, as an increased concentration by a factor ten for example leads to an increase by a factor ten in the number of observed DNA molecules on the surface, at least within a certain range where they do not saturate the surface.

The pH of the buffer solution and the surface treatment are related. If no surface treatment is done, DNA can be nicely stretched, but the concentration is low and the homogeneity is poor. Another problem is that the results are different with a fresh sample and with a sample over which lithographic structures have been designed. The reason is probably due to the PMMA

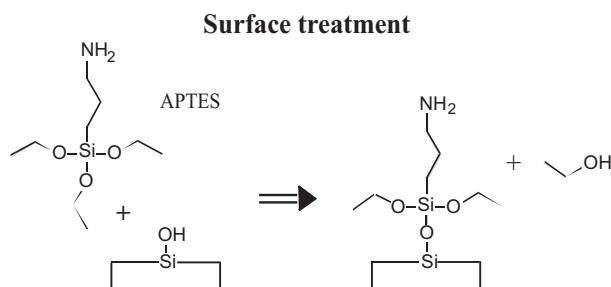


*Figure 4.4:* The APTES molecule binds to the silicon oxide surface by releasing at least one ethyl group. Then, depending on pH, the amino group will capture a proton and hence being positively charged. The mechanism is enhanced with lower pH.

used for the lithography and removed with acetone, but without letting a similar surface to the original one. If the surface is cleaned<sup>2</sup> but untreated, then there is almost no DNA on the surface, or very inhomogeneous if the concentration is increased. The reason is that there are almost no anchoring points. A way to provide them is to treat the surface with aminopropyltriethoxysilane (APTS or APTES) (see Fig. 4.4). A general review of this technique called silanization is given in Ref. [59]; it can also be used for a site selective placing of carbon nanotube on silicon oxide surface [60].

A uniform monolayer of APTES over the silicon oxide surface is delicate to achieve. The reaction binding between APTES and  $\text{SiO}_2$  is increased if the surface is cleaned with oxygen plasma or in an ozone environment, as the bonds are not saturated. Two methods were used to silanize the surface. With the first method, the sample is dipped in an APTES/toluene solution (typically 1/100 vol ratio, 10 min), rinsed in toluene and isopropanol and dried in an oven (10 min at  $100^\circ\text{C}$ ). With the other, the sample is placed in a small chamber with a glass container filled with 10 ml of a APTES/toluene solution (1/100 vol). The chamber is pumped for 10 s, and kept close for 1 min. A longer pumping time has to be avoided as it occasionally leads to the boiling of the solution and to drops projections over the sample. The sample is also dried for 10 min at  $100^\circ\text{C}$  in oven. The second method gave better results (better homogeneity and reproducibility) probably because in an APTES atmosphere the likelihood of binding between APTES molecules themselves is lower than in solution: the situation in Fig. 4.4 shows a case

<sup>2</sup>Typically with a 2 min process of oxygen plasma in a Reactive Ion Etching, see Appendix A for details

where one ethoxy group binds to the surface, but the two others can bind also to surface (ideal) or bind to other APTES molecules, leading to an agglomeration of molecules<sup>3</sup>. The rate of success of this method is however also variable.

The same problem as the one encountered with a too long deposition time can happen if the number of anchoring point is too large. One can reduce the number of anchoring points by reducing the coverage of APTES, i.e. typically reducing the concentration or deposition time, but it often leads to non-uniform coverage. One can also increase the pH of the deposition solution, hence reducing the charge of the amino layer. The second is easier to handle.

A study of the length of the molecules as a function of the surface treatment reveals quite large differences on length (see Fig. 4.5). Without RIE cleaning before the APTES covering, the average length is 23.4  $\mu\text{m}$ . With RIE cleaning before the APTES covering, the average length is 17.6  $\mu\text{m}$ . If one recalls Hooke's law (Eq. 4.3) and assume a contour length of 16  $\mu\text{m}$  for the DNA, one can calculate the force applied during the stretching. For a measured length of 23.4  $\mu\text{m}$ , this force is around 150 pN, and for a measured length of 17.6  $\mu\text{m}$ , this force is around 25 pN. It is however to note that different values for the contour length of stained DNA can be found in the litterature: 21  $\mu\text{m}$  [61], 20  $\mu\text{m}$  [56] or 16.1  $\mu\text{m}$  [62], all with the same dye and with same dye-base pairs ratio as we have. This has naturally an influence on the calculated force. We calculate with a value of 16  $\mu\text{m}$  for the unextended length, as a value of 20  $\mu\text{m}$  would be in disagreement with measured lengths of 17-18  $\mu\text{m}$ .

From the DNA contour length statistics, it is reasonable to say that the DNA are stretched most of the time as single molecules. At the highest resolution, one CCD pixel corresponds in our set-up to a size of 54.2 nm. So the resolution cannot give any information on the width of the DNA to determine if it is a single one or a bundle. We use also an atomic force microscope (AFM) to confirm that we indeed observe single molecule, as shown in Fig 4.6. The  $\text{SiO}_2$  surface is quite rough compared to the diameter of a single DNA strand. The scan profile shows however a maximum height around 1.4 nm, what is smaller than the expected diameter value of 2 nm.

---

<sup>3</sup>Ellipsometry measurements show that the thickness of APTES is around or below one monolayer (limit of resolution), but without information on the homogeneity of APTES layer [47]

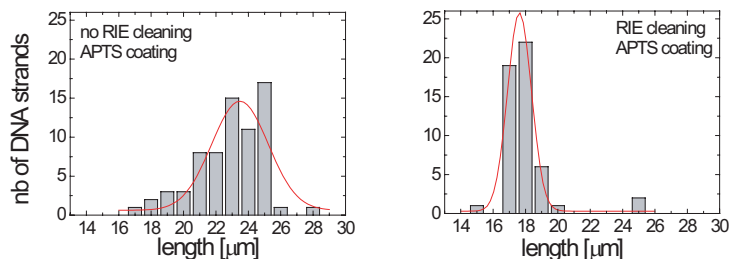


Figure 4.5: Difference in length as a function of the surface treatment: average length are  $23.4 \mu\text{m}$  (left)  $17.6 \mu\text{m}$  (right).

A reason for this effect can be attributed to the molecule compliance on the surface [63].

**Localized anchoring** Combined with this stretching method, other techniques were applied to anchor more site specifically the DNA. One is using the specific binding between streptavidin and biotin, but it is not so convenient with our requirements. The reason is that streptavidin itself needs to be specifically placed, what is done via angle argon sputtering on a slit full of streptavidin, but the binding with biotin is then not working properly. Another way is the design of a line in PMMA with e-beam lithography and evaporation of APTES in this line. After removal of PMMA in acetone remains a line of APTES. That is the advantage of APTES over streptavidin, because APTES does not seem to be affected by acetone while streptavidin is. Stretching can be achieved with such a line, as shown in Fig. 4.7. When stretching DNA over a structure, it is observed that on an aluminium line, the binding can also be specific, but again with quite poor reproducibility (Fig. 4.8). Since the poor reproducibility seems to be a general feature of this kind of site specific binding, we decide to apply a very different technique of positioning, as presented in the next section.

### 4.1.3 Summary

The hydrodynamic stretching method works nice on naked surface. The Fig. 4.9 shows typical results obtained under various conditions. On surfaces with designed structures, typically gold electrodes, the stretching is perturbed by those structures. Most of the time, the goal of spanning the

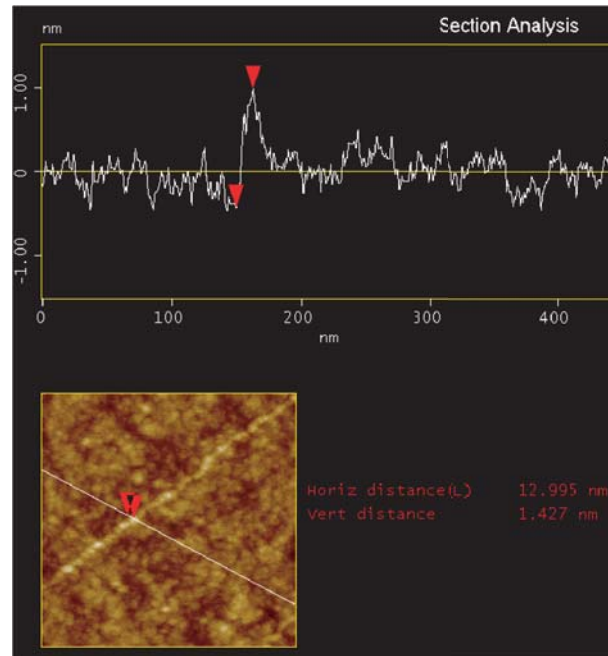


*Figure 4.6:* AFM picture of a  $\lambda$ -DNA molecule on a  $\text{SiO}_2$  surface treated with RIE and APTES. The profile show a height around 1.4 nm.

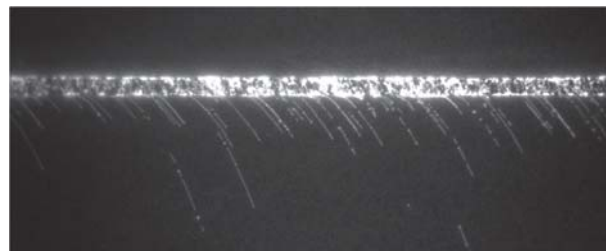


*Figure 4.7:* A line of APTES (designed with e-beam lithography) and stretching of DNA on it. One sees that the binding is very specific. The width of the picture is 170  $\mu\text{m}$ .

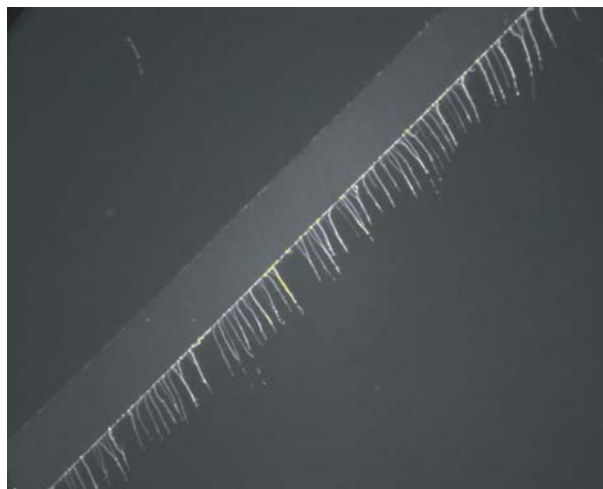


*Figure 4.8:* A line of aluminium designed by e-beam lithography and DNA stretched on it. The binding is quite specific on this picture, but not so reproducible. The width of the picture is  $170\ \mu\text{m}$ , the width of the Al-line is  $17\ \mu\text{m}$ .

electrodes is however reached (see Sec. 4.3 for further pictures). A comparison of this method with the electric field method is given at the end of Sec. 4.2.

## 4.2 Electric field orientation and positioning

### 4.2.1 Mechanisms

Another technique to manipulate the DNA strands in solution is the use of an electric field. Under slightly basic conditions, the phosphate groups within the backbone deprotonize and the DNA is negatively charged. Electrophoresis uses this charging effect to sort out DNA or other proteins as a function of their length by applying a dc electrical field. Note that the effect is not as trivial as it first looks like. The charge of the DNA depends linearly on the length, and so does the electric force, but the drag force also depends on its length. Consequently the speed of the molecule is expected to be length independent. To sort out molecules as a function of their size, a gel has to be used, because longer molecules are slower in a gel than short ones. It is also a common use to add extra charge to the molecule with SDS for example (sodium dodecyl sulfate) [8]. The necessity of the gel makes however elec-

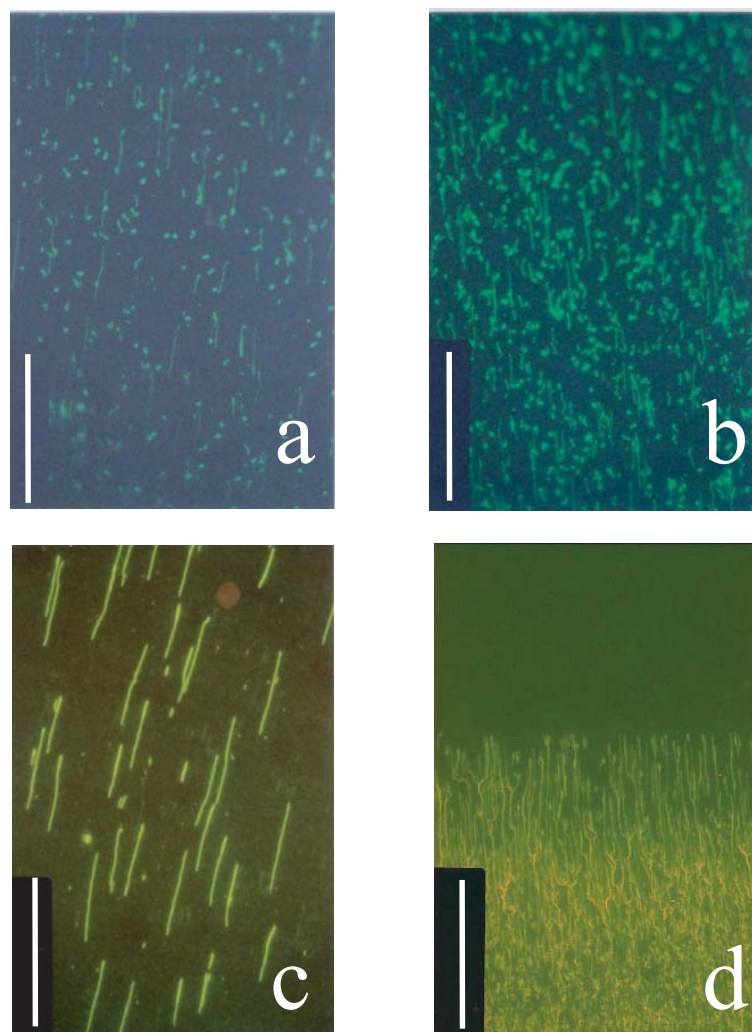


*Figure 4.9:* Typical results for hydrodynamic stretching of  $\lambda$ -DNA molecules. The scale bar is  $40\ \mu\text{m}$  on all pictures.

(a) Concentration is  $2\ \mu\text{g}/\text{ml}$ ,  $\text{pH} \approx 7.5$ , (b) Concentration is  $10\ \mu\text{g}/\text{ml}$ , same  $\text{pH}$  as (a). One sees that there are some unstretched DNA strands (appearing as dots).

(c) Concentration is  $2\ \mu\text{g}/\text{ml}$ ,  $\text{pH} \approx 9$ , (d) Meniscus line on top of the solution: on this sample, the APTES concentration is too high, and too many DNA bind without being stretched.

trotophoresis unusable for our purpose. It is also possible to align  $\lambda$ -DNA in a dc electrical field [64], but it seems only possible if the DNA is previously anchored at one end, otherwise the whole DNA would move, but not unwind.

We used a method where an ac-electrical field is applied between metal electrodes. The manipulation of the DNA is based on the interaction of the induced dipole moment in DNA and the applied electric field. We designed electrodes in such a way that a reduced number of molecule can be positioned and anchored at a predetermined position, contrary to similar experiments described in [65, 66].

When placed in solution and exposed to an inhomogeneous field, the DNA undergoes two effects. One is a torque that aligns the DNA with the field, the other is a dielectrophoresis force which drives the DNA in the direction where the electric field is the strongest [67]. This situation is called positive dielectrophoresis and it occurs when the polarizability of the molecule in solution is higher than the one of the medium. Otherwise it is called negative dielectrophoresis. Both effects depend on the polarizability  $\alpha$  of DNA, that is supposed to be strongly affected by the counterions clouds around it in solution. For a neutral object in a non uniform field, the dielectrophoresis force can be written as

$$\vec{F}_d = \vec{p} \cdot \vec{\nabla} \vec{E} = \alpha \vec{E} \cdot \vec{\nabla} \vec{E} = \frac{\alpha}{2} \vec{\nabla} (E^2) \quad (4.4)$$

where  $\alpha$  is the polarizability of the object,  $\vec{p}$  is the induced dipole moment ( $=\alpha \vec{E}$ ) and  $\vec{E}$  is the local electric field.

The polarizability  $\alpha$  can be written as  $\alpha_V V$ , where  $\alpha_V$  is the polarizability per unit volume and  $V$  the volume. To describe what happens in a solution, Eq. 4.4 has to take into account the permittivity of the solution, so the polarizability per unit volume is given by [68]

$$\alpha_V = \frac{\epsilon_0 \epsilon_1 (\epsilon_2 - \epsilon_1)}{\epsilon_1 + A(\epsilon_2 - \epsilon_1)} \quad (4.5)$$

where  $\epsilon_1$  is the permittivity of the medium,  $\epsilon_2$  the permittivity of the molecule and  $A$  a geometrical factor ( $A$  varies from zero to one :  $A=1/3$  for a sphere and  $A=1$  for a short rod).

As  $\epsilon_2$  is much larger than  $\epsilon_1$  in the case of DNA in water [69], the Eq. 4.5 can be simplified and one can write the force as

$$\vec{F}_d \approx V \epsilon_0 \epsilon_1 \vec{\nabla} (E^2) \quad (4.6)$$

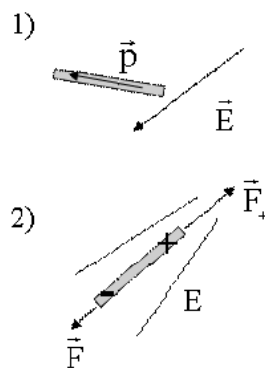


Figure 4.10: Scheme of the effects of an electric field on a rod.

(1) Alignment torque of the dipole with the field (2) Dielectrophoresis force in the direction where the field is the strongest.

A rough estimation of the electrical field value  $E_{th}$  necessary to overcome thermal fluctuations can be obtained by integrating Eq. 4.6 over distance and comparing the result with  $k_B T$ :  $E_{th} \approx \sqrt{k_B T / (r^2 l \epsilon_0 \epsilon_1)} \lesssim 10^7$  V/m, showing the necessity to use relatively high electric field. The force considered here is the one exerted on one segment of the DNA molecule, as each segment undergoes thermal fluctuations. The value of length  $l$  is thus the persistence length, 100 nm. The other values are the radius  $r = 1$  nm and the permittivity of water, 80.

The second effect is the alignment of the molecule with the field. As DNA can be seen as a chain of rigid segments, the aligning effect will act on each of them, resulting in a completely aligned molecule, except if nodes are forming. The torque on each rigid part is given by

$$\vec{M} = \vec{p} \times \vec{E} \quad (4.7)$$

The molecule undergoes a stretching force which can be estimated in a rough approximation by the sum of the opposite electrostatic forces  $F = \pm q \cdot E$  exerted on both ends of the molecule. The charge is given by  $p/l$ , where  $l$  is the length of the molecule. A value of  $10^5$  D was obtained for DNA molecules about  $1.5 \mu\text{m}$  long [69]. The force is then around 0.2 pN for an applied field of  $10^6$  V/m, one or two order of magnitude smaller than forces present with the hydrodynamic stretching method. It is in agreement with the experiment of Washizu, who measured no extension of DNA ac-field technique [65].

### 4.2.2 Experiments

The experiment is performed as follows. Electrodes are structured on a 2cm\*2cm wafer (see Appendix A for details) and contacted to a voltage source. As mentioned above, fields in the order of  $10^7$ V/m are required. The easiest way to achieve such high field is to have quite near electrodes, typically a few micrometers apart, so that voltages of several volts are enough. The set-up is such that it is possible to simultaneously run the stretching and observe the sample (see Appendix B). A volume of 5 to 10  $\mu$ l of DNA solution<sup>4</sup> is deposited between the surface with the electrodes and a glass cover slip. A certain time is needed before the liquid does not move anymore. Then the voltage is gradually increased until the DNA start to accumulate between the tips of the electrodes, where the field is the strongest. It typically occurs at 2 or 3V. When the field is suppressed, some DNA are released to the solution and some remain attached to the tips. During this procedure, a sequence of CCD pictures is recorded (1 picture per second). The accumulation of the DNA at the end of the electrodes tips is schematically shown in Fig. 4.13. The Fig. 4.12 is the last picture of the recorded sequence.

The technique operates between a few kHz and a few MHz, with a good efficiency of the trapping process around 1 MHz. A high frequency is a great advantage since it helps limiting electrochemical effects by lowering the potential drop at the electrode-solution interface. To prevent any low-frequency contribution, a high pass RC filter is used. A typical example of what can happen otherwise is shown in Fig. 4.11.

With electrodes as shown in Fig. 4.12, no turbulence effect is observed. The Joule heating is estimated as follows. The power per volume dissipated by a field  $E = 10^6$  V/m in a solution with conductivity  $\sigma = 70$   $\mu$ S/cm is given by  $\sigma E^2 = 7$  W/ $\mu$ l. In adiabatic conditions, this would result in an almost instantaneous evaporation of the solution. Since the field is very intense only close to the electrodes, only a limited volume is heated. The heat is then dissipated in the whole solution. The heated volume is estimated to  $(5 \cdot 20 \cdot 10) \mu m^3 = 10$  pl, so the power deposited is  $7 \text{ W} \mu\text{l}^{-1} \cdot 10 \text{ pl} = 7 \cdot 10^{-5}$  W. The temperature raise per second is given by  $\Delta Q/mct \approx 3$  mK/s, where  $m$  is the mass of the whole volume of solution, 5  $\mu$ l,  $c$  is the specific heat of water and  $\Delta Q/t$  the deposited power. A good thermal coupling of the device to the sample holder further helps to limit heating effects.

Note that without a careful design of the electrode and choice of the buffer

---

<sup>4</sup>DNA at a concentration of 1 $\mu$ g/ml in MES buffer  $\sigma = 70$   $\mu$ S/cm, pH 4.1

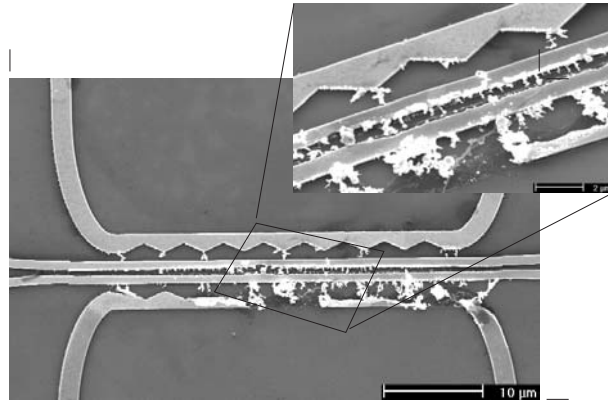


*Figure 4.11:* Example of electrodes destroyed during the ac-field technique.

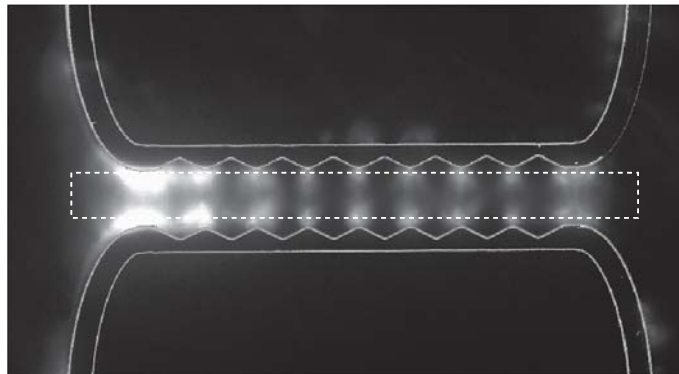


*Figure 4.12:* A fluorescence picture of ac-stretched DNA. The border of the electrodes (in this setup only two) are artificially enhanced. In the middle, a region of interest (ROI) is selected for the calculation of mean intensity (see Fig. 4.13)

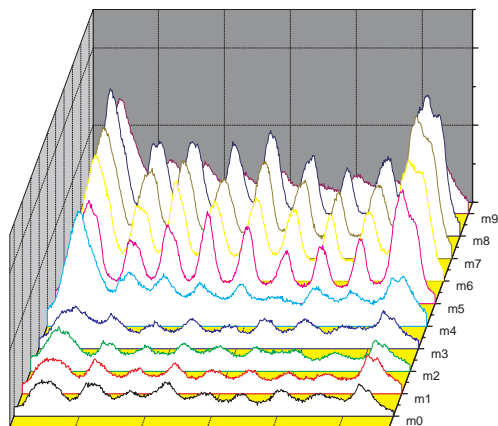


*Figure 4.13:* Ten successive plots of the intensity [a.u.] recorded every second over the ROI selected on Fig. 4.12. A mean value of the intensity recorded by the CCD is calculated for every vertical line of the ROI and then plotted as function of position along the electrodes. The field is applied between the measurements m3 and m8. The measurements m9 corresponds to the image shown on Fig. 4.12, i.e. after the release of the field.

solution, the experiment can not be performed successfully. The Fig. 4.14 shows a different structure and pictures of what is happening when a field is applied. The right angle of the electrodes as well as a too conductive buffer<sup>5</sup> lead to too high currents in the solution. The consequences are turbulence flows and/or even destruction of the electrodes.

### 4.2.3 Summary

Both techniques, hydrodynamic stretching and ac-stretching, have their advantages and disadvantages, which have to be considered as a function of what has to be measured afterwards. The Table A.1 compares the two methods and the used parameters for each of them. The Fig 4.15 shows four pictures of the result of stretching experiments on surfaces with electrodes: those samples (except the (a)) are ready to be measured.

<sup>5</sup>Same buffer as for hydrodynamic stretching, i.e. Tris, pH 10 and 1 mM NaCl,  $\sim 800 \mu\text{S}/\text{cm}$

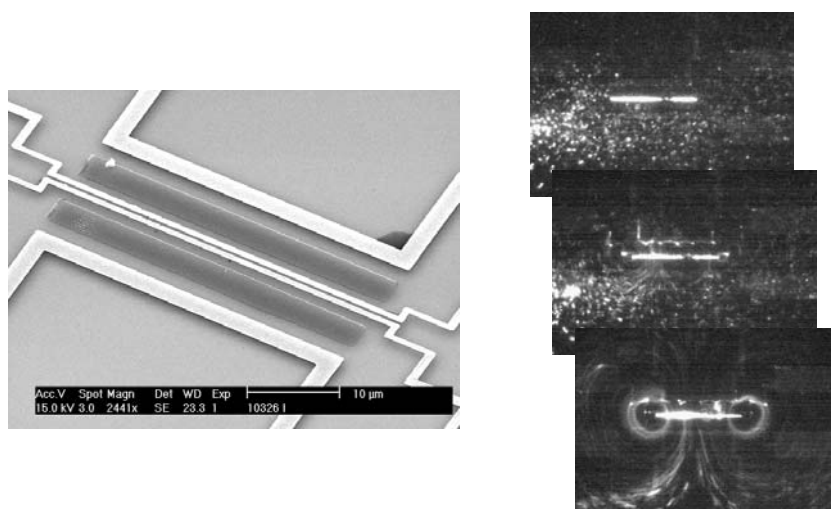


*Figure 4.14:* A SEM picture (left) and three fluorescence pictures (right). On the SEM picture, one sees the two outer electrodes, used to apply the ac-field, two squares of aluminium, and two inner electrodes for further electrical characterizations. The purpose of the aluminium line is to provide a stronger anchoring site for the DNA (see Fig. 4.8 or ref. [70]). The three fluorescence pictures show a turbulence effect due to a too high temperature.

	hydrodynamic stretching	ac-stretching
buffer	TRIS-EDTA-NaCl (10-1-10 mM) pH 8-9, 1-10 $\mu\text{g}/\text{ml}$	MES pH 4.1, 1 $\mu\text{g}/\text{ml}$
parameters	150 $\mu\text{m}/\text{s}$	0.5-1 MV/m, 1 MHz
advantages	usable on various structures lot of DNA stretched (of measurable length) post-staining faisable	precise positioning soft stretching  observable in situ
disadvantages	not very homogeneous strong stretching forces	binding may be weak

*Table 4.1:* Comparison of the two positioning methods

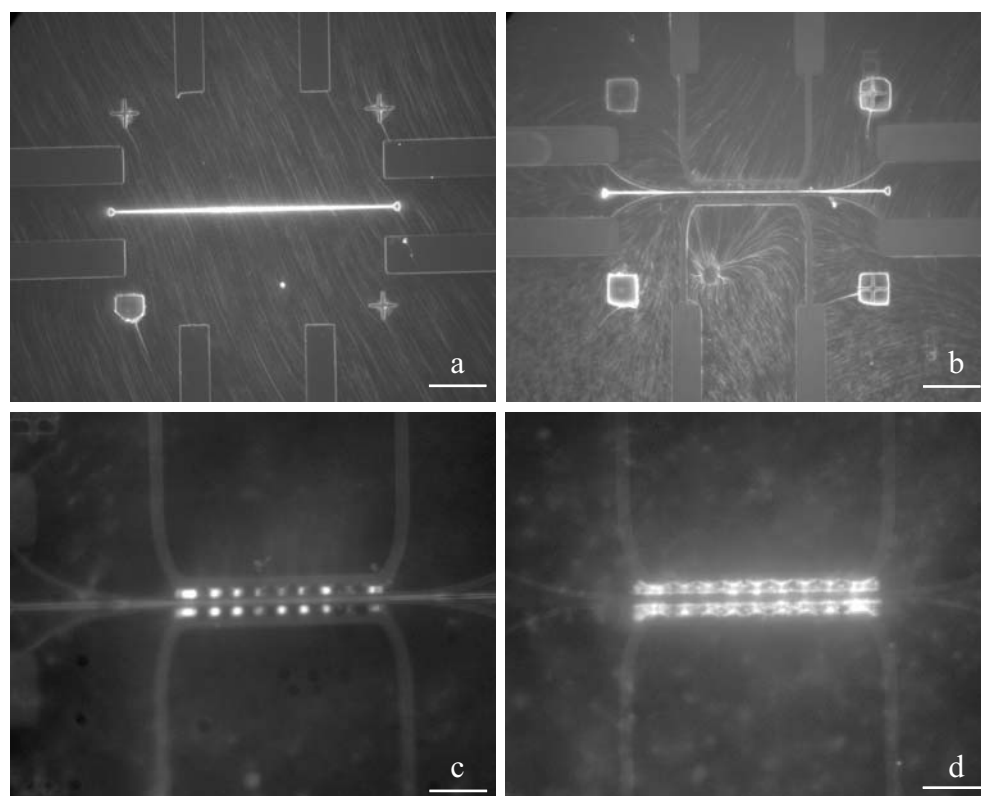


*Figure 4.15:* Four fluorescence pictures to compare hydrodynamic stretching (a and b: scale bar is 20  $\mu\text{m}$ ) and ac-stretching (c and d: scale bar is 10  $\mu\text{m}$ ).

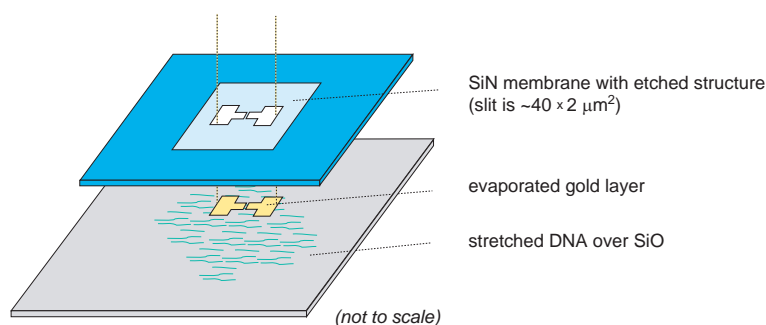


Figure 4.16: Scheme for the evaporation of contact electrodes on top of previously stretched DNA.

## 4.3 Conductivity measurements

The ultimate goal here is to characterize a single molecule, and not an ensemble like fibers as presented in Chap.3. It is reasonable to have first the middle term goal to measure several single molecules in parallel, thus enhancing the probability to catch well contacted, undamaged candidates. Care has also to be taken that the instrument used to check the presence of DNA does not damage it or induce artefact. We explore different methods and different structures to contact the DNA.

### 4.3.1 Electrodes on top

Some experiments are done with electrodes on top of DNA, with the risk that DNA might be destroyed by the evaporation of the electrodes. This technique is a standard one to contact carbon nanotubes, but those are known to be much more robust than DNA, as they are not damaged under an electron beam or in commonly used chemicals like PMMA, acetone, etc. The method used is the following. First DNA molecules are stretched over flat  $\text{SiO}_2$  surfaces with the hydrodynamic method. Typically three samples are run in parallel, one with stained DNA for immediate observation, another one with stained DNA and one with unstained DNA. Then gold electrodes are evaporated on top of the two last samples through a mask designed previously in a  $\text{SiO}_2$ - $\text{Si}_3\text{N}_4$  membrane. The membrane is put with its face down to the surface to have the smallest possible distance between the two surfaces, thus the distance is restricted only by dust particles between them. An example is shown in Fig. 4.17.

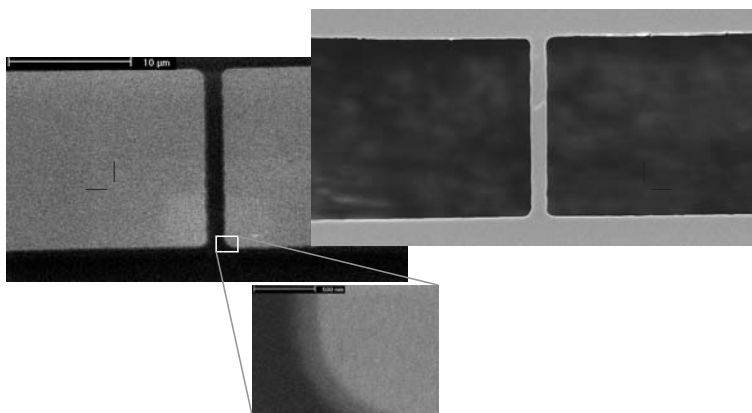


*Figure 4.17:* The mask (right, in grey), the evaporated electrode (left, in grey) and a magnified view of a sufficiently sharp border

The problem encountered with this technique is its low reliability, mostly due to the fact that one cannot clean correctly the mask, as the membrane is destroyed in an ultrasonic bath. Randomly deposited dust particles can then be responsible for unsharp evaporations. The Fig. 4.18 shows the geometry of the evaporation: the metal source (1 cm diameter) is 40 cm away from the target. Particles with a diameter of  $80 \mu\text{m}$  between the sample and the mask membrane are large enough to be responsible for a shadow edge of  $2 \mu\text{m}$ , what results with a bridge between the two electrodes if they are closer than  $4 \mu\text{m}$ .

The conductivity measurements in these conditions give no conduction through the sample. Due to the difficulties explained above and to the fact that evaporation may damage the DNA, few experiments have been done. Another reason is also that it is difficult to control the presence of DNA after the evaporation, because the dye is not visible anymore, and the post-staining give no clear results.

### 4.3.2 Molecules on top

The other possibility is to pattern the electrodes first and then to position the DNA on top of them. Experiments with carbon nanotubes show that the electrical contacts are lower in this case [71], but contact resistances up to  $1 \text{M}\Omega$  are still acceptable for DNA. Different configurations were realized and

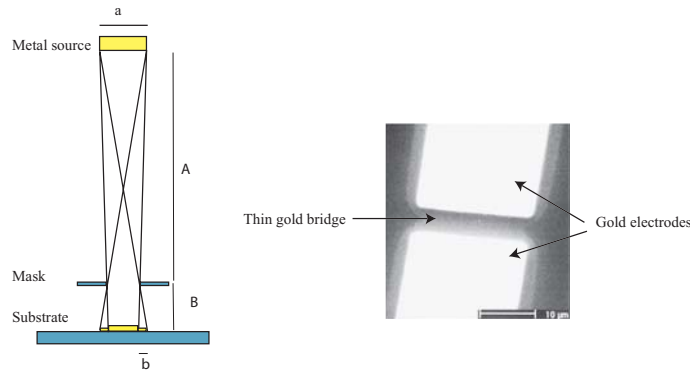


Figure 4.18: Left) The geometry of the evaporation:  $A/a = B/b$ , where  $a=1$  cm,  $A=40$  cm,  $b=2$   $\mu\text{m}$  on the right image, thus  $B = 80\mu\text{m}$ )

Right) SEM image: a bridge of gold connects the two electrodes. The device has a resistance of a few Ohm.

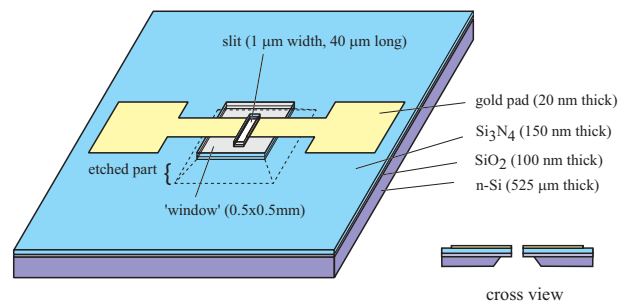


Figure 4.19: The sample holder with the membrane. DNA has to cross the slit designed in the center

will be discussed.

**Set up for LEEPS microscope** The first set-up was designed in such a way that one could check the presence of DNA crossing the electrodes with the LEEPS microscope and eventually get some temperature dependent measurements and noise measurements in a cryostat, if possible. For that purpose, it needed to be transparent at the place where the DNA would span the electrodes. A sketch of it is given in Fig. 4.19, SEM pictures in Fig. 4.20 and how it was mounted in the LEEPS microscope in Fig. 4.21.

Due to the extreme fragileness of the membrane, this kind of structure was not further developed.

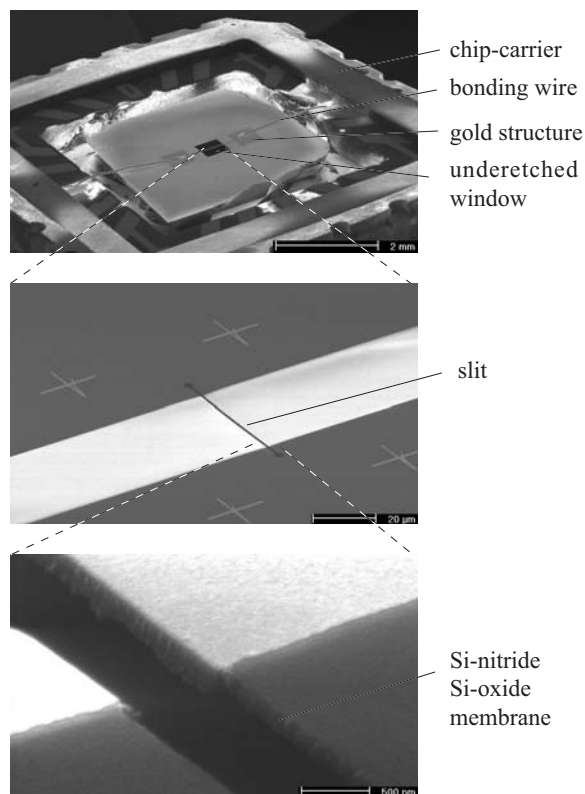


Figure 4.20: SEM pictures of the sample holder mounted on a chip carrier (also drilled in its middle)

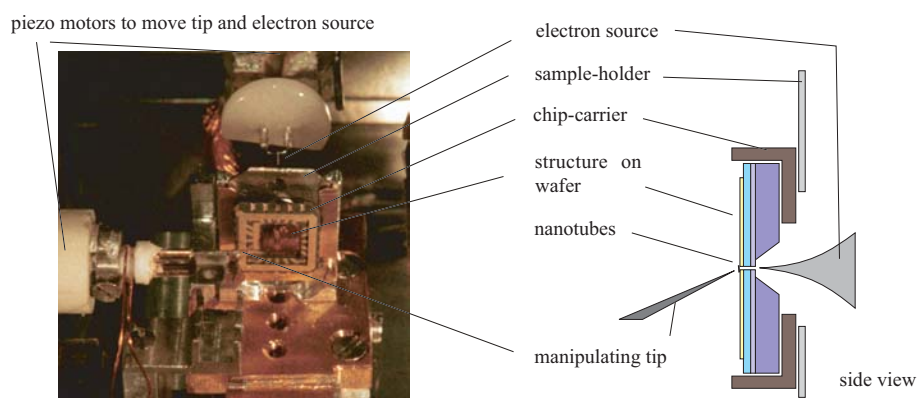


Figure 4.21: The chip carrier in the LEEPS microscope

**Flat structures** The easiest way is to pattern electrodes on a flat surface. The advantage is the possibility to test the presence of DNA with fluorescence microscopy. The samples are also robust enough to be used several times with careful cleaning<sup>6</sup> between each experiments. Different distances between the electrodes are tested (from 200 nm to 5 microns), as well as different materials (Ti/Au or Ti). The size (length and width) of the electrodes are also varied, sometimes increased to increase the chance to capture DNA, sometimes decreased to have better control on the sample under test.

A typical measurement is shown in Fig. 4.22. As the resolution current at low frequency is around 20 pA for 2 V, the resistance of the device is larger than 100 G $\Omega$ .

Around sixty experiments were performed on similar structures or slightly different ones with the ac-field stretching method, with stained or unstained DNA. One measurement had a different behavior, as shown in Fig. 4.23. It was the only one for which control experiments of the structure showed no clear defects (see Sec. 4.3.4). The resistance was around 300 M $\Omega$ .

Around thirty experiments were performed with similar or different structures with the hydrodynamic stretching. None of them showed any current above resolution with the presence of stained or unstained DNA. Two examples of pictures are shown on Fig. 4.24. The picture (a) is an example of lots of DNA stretched over Ti electrodes. The picture (b) is an example of few DNA stretched over Ti/Au electrodes. The typical sample as shown in Fig. 4.15 were also insulating.

**Flat structure with trench** We also designed structures with flat electrodes but with a trench between the two inner electrodes. This kind of structure is presented in Appendix A as an example of a structure requiring different techniques for its fabrication. No measurable current were obtained with this structure either, with stained or unstained DNA. It shows that suspended DNA are as insulating as DNA adsorbed on a surface.

### 4.3.3 Other parameters

As for fiber, the influence of an oxidizing agent like oxygen gas was also tested, without any noticeable difference on the measured current through the sample.

---

<sup>6</sup>Ultrasonic bath in acetone, ethanol and water and ozone treatment

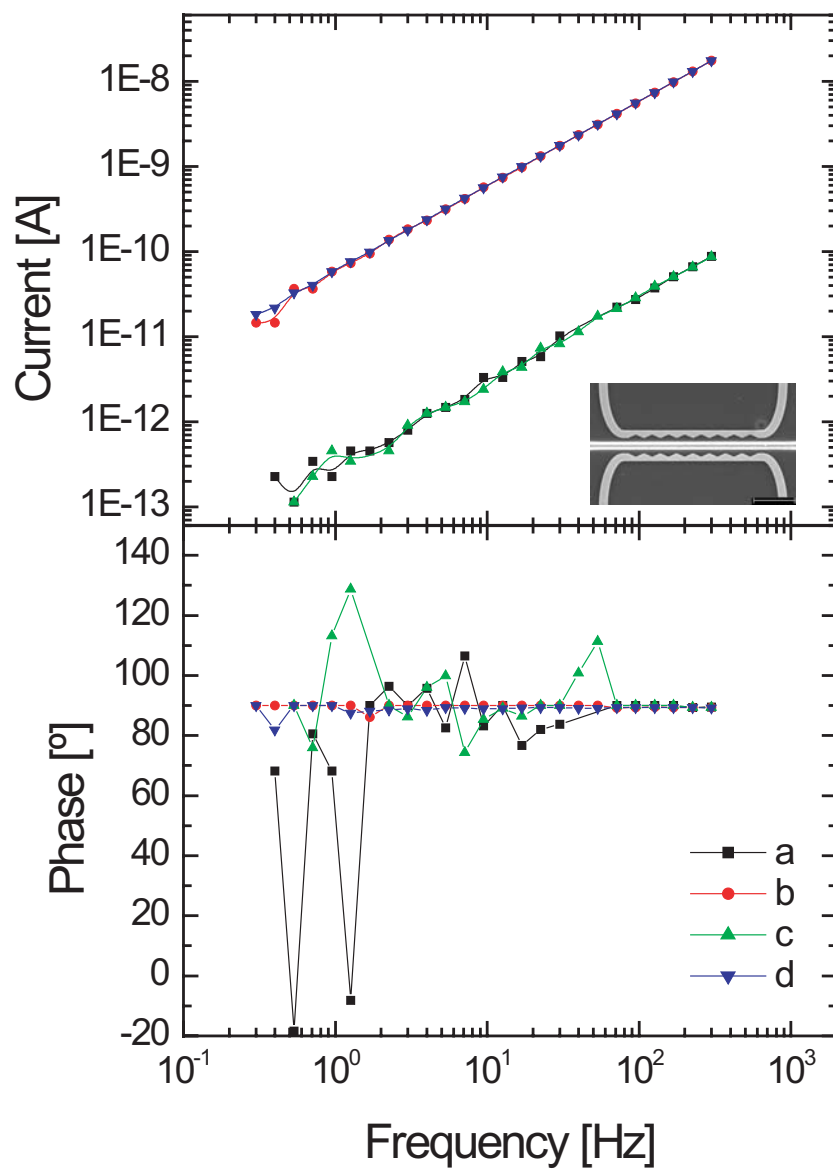


*Figure 4.22:* Typical measurements of DNA on the structure shown in inset (scale bar of SEM image :  $10\ \mu\text{m}$ ). The voltage is applied between the two inner electrodes.

a) (without) and c) (with) DNA at 0.01 V

b) (without) and d) (with) DNA at 2 V

The capacity is roughly 5 pF

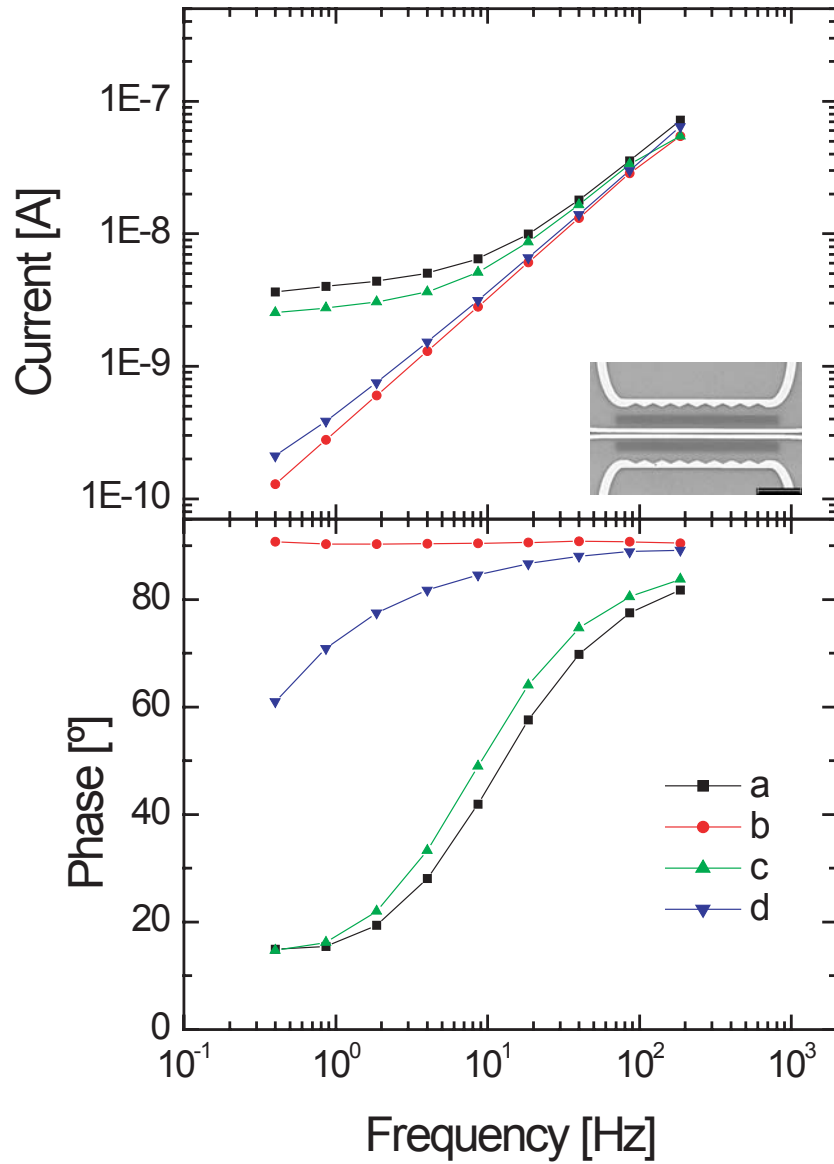
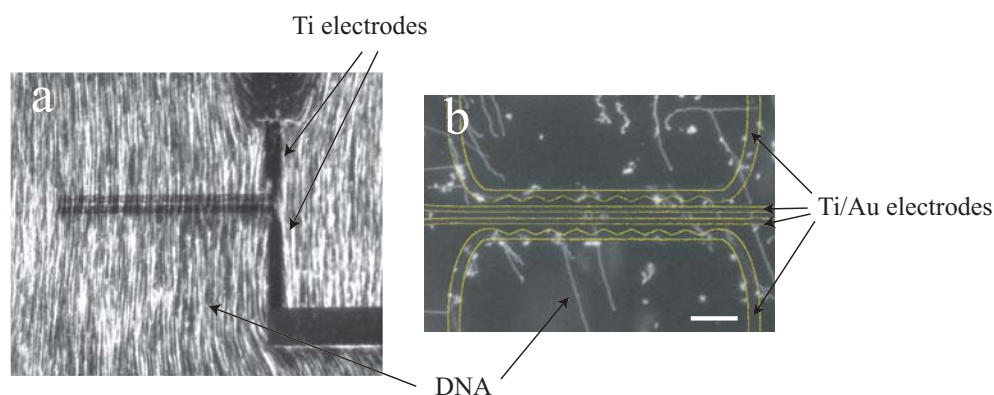


Figure 4.23: Measurements (at 1 V) of unstained DNA stretched on inset structure with ac-field (scale bar of SEM image :  $10 \mu\text{m}$ ). The two outer electrodes were used for the field stretching, and the curves are measured with voltage applied between the two inner curves.

- a) DNA in air: resistance at low frequency is  $250 \text{ M}\Omega$
  - b) DNA in vacuum (same curve as structure without DNA)
  - c) DNA in air again: resistance is  $400 \text{ M}\Omega$
  - d) DNA measured the next day
- The capacity of the device is  $50 \text{ pF}$



*Figure 4.24:* Two examples of DNA stretched with hydrodynamic flow and tested for conductivity.

a) DNA over Ti electrodes (length=70  $\mu\text{m}$ , gap=1  $\mu\text{m}$ , width=5  $\mu\text{m}$ ): one sees that over the electrodes, the DNA are still visible. That might be due to their high number, but also to bad contact to the metal.

b) DNA over Ti/Au electrodes (white scale bar is 8  $\mu\text{m}$ ). Note that those DNA are not stretched with electrical field, even if it is the structure commonly used for this.

The humidity level could only be tested on the sample who showed a resistance of 250  $\text{M}\Omega$  in air conditions. In vacuum, the current was below the resolution current, and once in air again, almost the same value for resistance was measured. Other samples showed no current, in air or in vacuum.

A study as a function of DNA with defined sequences, like poly(AT) or poly (GC), was not done, since long DNA strands are difficult to obtain for the typical distances of our set-up (minimum gap distance is around 0.3  $\mu\text{m}$ ). We tested however other DNA preparations and buffer solutions with different ions, sodium or magnesium, for the same reasons presented for fibers. A detail of the samples tried is given Appendix C. No measurable resistance could be obtained with those samples (stained or unstained DNA).

As DNA has a strong absorption peak around 260 nm, a property used for DNA concentration measurements. We illuminated therefore DNA with UV light to see if mobile charges can be excited. The risk is also that the DNA is destroyed before any current can be measured. No significative decrease of resistance could be related with the illumination of UV.

### 4.3.4 Controls

As with fiber, the measurement of the current as a function of the frequency indicates whether the device is resistive or capacitive. Calculations from graphs as shown in Fig. 4.23 and Fig. 4.22 give value for  $C$  of 50 pF and 5 pF respectively. An estimation of the capacity of the structure itself gives indeed values in the same range. For that, one has to estimate the surface of the electrodes (see Fig. 4.25). The total capacity is

$$C = C_1/2 = 1/2\epsilon_0\epsilon_r \frac{S}{d} \quad (4.8)$$

where  $S$  is the surface of the electrodes,  $d$  the thickness of the insulating layer and  $\epsilon_r$  its relative dielectric constant (around 4 for  $\text{SiO}_2$  or  $\text{Si}_3\text{N}_4$ ).

In Fig. 4.23, the surface  $S$  is roughly the surface of the contact pads (designed as  $C$  in Fig. 4.25) ( $\approx 2 \cdot 1 \text{ cm} \cdot 100 \mu\text{m}$ ) and  $d$  is  $0.5 \mu\text{m}$ . The calculated value of  $C$  is then of 70 pF. The ratio of the area  $B/C$  corresponds roughly to the ratio of the capacities, explaining thus the different values.

Each electrode is always contacted on its two sides, allowing thus to check that the absence of current cannot to be attributed to an accidental opening of the circuit. Resistances of  $50 \Omega$  are measured, what is the expected resistance of a piece of gold of 1 cm in length,  $50 \mu\text{m}$  in width and 80 nm in height, typically the dimension of one electrode.

An estimation of the contribution of an adsorbed water layer gives a resistance value of

$$R = \rho \frac{d}{lh} = 2 \cdot 10^5 \frac{0.5 \cdot 10^{-6}}{70 \cdot 10^{-6} \cdot 80 \cdot 10^{-9}} \simeq 10^{10} \Omega \quad (4.9)$$

where  $\rho$  is the resistivity of water and  $d, l, h$  are the dimensions of a water layer that would contact the two central electrodes (width, length and height respectively).

This is an estimation for a case where the height would be the same as the one of the electrodes, 80 nm. A more reasonable value would be probably hundred times smaller, hence the resistance would be hundred times bigger (if the formula is still valid for such a thin layer, but at least it allows an estimation). However, as  $100 \text{ G}\Omega$  is also the maximum resistance we can measure with the set-up (see Fig. 4.22), we do not need to worry about

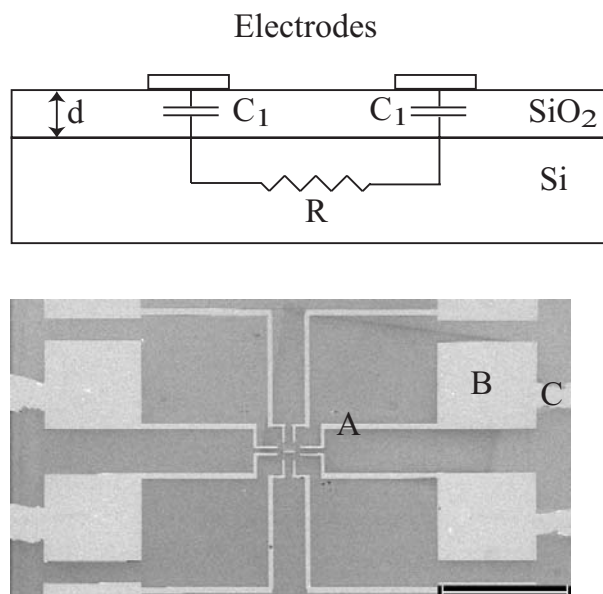


*Figure 4.25:* Scheme of the capacity of the structure.  $C_1$  is the capacity of the insulating layer,  $R$  is the resistance of the silicon (small, as the silicon is p-doped).

The scale bar on the SEM picture is 0.5  $\mu\text{m}$ . The area A is neglected. The area B is the contact pads for structures designed for hydrodynamic stretching. The area C is only present for structures designed for ac-field stretching: these are large contacting pads of roughly  $1\text{cm} \times 0.1\text{cm}$

the presence of such a water layer. If the sample is still covered with a visible water layer, a resistance in the  $\text{M}\Omega$  is measured. The current however disappears once the sample is in vacuum and does not come back when measured in air again, on the contrary with what was observed in Fig. 4.23.

## 4.4 Conclusions

All the experiments performed on devices with single molecules showed no measurable current, with a minimum resistance around  $100\text{ G}\Omega$ . One exception showed a resistance of  $250\text{ M}\Omega$ . Due to the singularity of the event, we could not make refined controls like checking if this current disappears if dipped in a solution with DNA digestion enzymes as done in Ref. [39].

The quality of the contacts between the electrodes and the molecule under study was shown to be a decisive parameter. People observed resistances

---

at least four order of magnitude smaller for molecules chemically bounded to the electrodes [72]. Although we cannot guarantee high quality contacts in our experiments, some clues tend to show they might be reasonably good. The first one is the observation of the quenching of the fluorescent dye over the electrodes. This quenching is due to the energy transfer of the excited electron in the dye to the metal underneath. The efficiency of this quenching is proportional to  $r^{-6}$  where  $r$  is the distance between the dye and the quencher [73]. Conversely, we observed a weaker quenching when a lot of DNA are spanning Ti electrodes. The second clue is that no larger current is measured, in the case of ac-field stretching, between the two outer electrodes. As the dielectrophoresis drives the molecule to those electrodes, one might expect a better contact between them and the molecule. One should however say that the nature of this contact is also unknown.

For the majority of the measurements, the resistance of the device is larger than 10 G $\Omega$  for structures with large pads and larger than 100 G $\Omega$  for structures with small pads. As several molecules are connected in parallel, the resistance of one molecule must then to be multiplied by the number of molecules, assuming they have all the same contact resistance. This number can be estimated around 10 for the ac-field stretching and up to 50 for hydrodynamic stretching, leading to even higher value of resistance per single molecule.



# Chapter 5

## Conclusion

We have been exploring the DNA electric transport properties over large distances: 0.2 to 5  $\mu\text{m}$  for the single molecules experiments, and up to millimeter for the fiber experiment. The fiber experiments showed that the humidity level is the dominant parameter for the conductivity measurement.

The experiments with single molecules required first a careful and reliable technique for the physical manipulation of the DNA, what could be successfully achieved. The electric measurements showed that the lower limit of the device resistance is to be attributed to the set-up used to position and measure the DNA. The set-up used with the stretching of DNA by a recessing meniscus lead to a resistance larger than 100  $\text{G}\Omega$ , and the one for the positioning of DNA with an ac-field lead to a resistance larger than 10  $\text{G}\Omega$ . The question whether DNA can be used for producing electronic devices gets, in these conditions, a negative answer. This is in agreement with recent publications whose conclusions are also that  $\lambda$ -DNA is insulating [74, 75].

If 'bare' DNA cannot be used as a molecular wire, are there still possible applications in electronics? The answer to this question is probably yes. Different approaches are conceivable. One is to chemically modify the DNA to modify its electronic properties, as presented in Ref [76] where metallic ions are chemically bonded insides the bases, leading to a metallic behavior of the ropes. Another approach is to use the DNA as a template for building metallic wires, as presented in Chapter 2. The actual trend is to consider molecular electronics not just as the fabrication of devices with conducting molecules, but also as the use of the molecular organization properties. For this so-called bottom-up approach, the future of DNA molecules is guaranteed.



# Appendix A

## Structuring Techniques

This appendix gives a glimpse of the techniques used to fabricate the desired structures for measuring the DNA molecules. Those techniques are commonly used in mesoscopic physics, where typical design's dimensions are in the order of microns. It is essentially the transposition of a flat structure over a surface, with sometimes small (below microns) 3d extension.

### A.1 Electron-beam lithography

Lithography is the general name for a process where a pattern is transferred on a substrate. Originally one uses a stone (lithos) with the design on it, dips it in ink and press it on a substrate to write (graphein) the pattern. Now it also refers to other methods, like photo or e-beam lithography. In both cases, the surface to be patterned is covered with a resist (usually organic polymers) whose exposition to light or electrons will change the solvability in a developing solution. In the case of positive (negative) resist, the exposed (unexposed) area will dissolve. In photolithography, light with short wavelength is used to illuminate the sample through a pre-designed solid mask. This method is fast (the exposure time is independent of the surface area) and the apparatus is relatively cheap and easy to use. The limitation to the resolution is mainly given by the wavelength of the used light.

To achieve higher resolution one needs higher energy beams, and a scanning electron microscope (SEM) is a standard machine used to make e-beam lithography. The pattern is designed on a computer that transfers it via the scanning mechanism of the microscope. The resolution is mainly restricted

by the size of the beam and the control of the proximity effect. This phenomenon is due to backscattering of electrons by the surface and that make the structure bigger: if this can be an advantage in order to have a good undercut profile, it reduces the possible size of two adjacent structures. One can reduce this undesirable effect by reducing the dose of electron on sensitive places. E-beam lithography is especially convenient for research where structures must be changed very often. The disadvantage is that a certain dose (number on electrons per surface area) is needed for developing with the consequence that the needed exposure time increases with increasing surface area. For high resolution, one has to work with low current (i.e. small spot size) and high magnification, and for bigger structure one can work with bigger current to reduce exposure time. In the group, the SEM used is a *JEOL JSM:IC848* working with an acceleration voltage of 35 kV. It is also equipped with an external compensation of environmental magnetic field. The program used to design and transfer the structure is *ELPHYQuantum*, from the firma *Raith*. With standard positive resist (PMMA, polymethylmethacrylate 950 K, from *Allresist*), the electron beam cuts the polymer strands in small pieces, hence the higher solvability in developer, a solution of MIBK/IPA (4-Methyl-2-pentanone and 2-propanol) in 1/3 volume ratio. Pure IPA is used as stopper. The resist now acts as a mask for metal evaporation, etching or spinning of solution.

## A.2 RIE and wet chemical etching

A possibility to give a 3d extension to a structure is to do some etching, i.e. removal of materials. This can be done by sputtering (pure physical action), Reactive Ion Etching (RIE) (physical and chemical actions) or wet etching (pure chemical action). The RIE is done in a *PlasmaLab 80 plus*, from *Oxford* (see Fig.A.1). A gas is introduced in a chamber where a high frequency field is applied between a table and the chamber's wall. The few ions in the gas (due to outer radiation) ionise the others by an avalanche process, leading to a glowing plasma. The voltage drop near the surface accelerate the ions perpendicularly to the surface where they chemically react with it. The desired parameters (kind of gases, pressure, voltage) are determined mostly empirically.

A pure chemical etching can be done in an appropriate solution. The solution used in this work etches  $\text{SiO}_2$ , but almost not silicon. The advantage

Purpose	Gas [sccm]	Power	Typical time
Oxygen plasma (cleaning)	O <sub>2</sub> ,16	100W	2min
Si <sub>3</sub> N <sub>4</sub> and SiO <sub>2</sub> etching	CHF <sub>3</sub> , 34; O <sub>2</sub> ,4	80-100W	30nm/min

Table A.1: Parameters for the plasma treatment (all at a pressure of 0.025 mTorr)

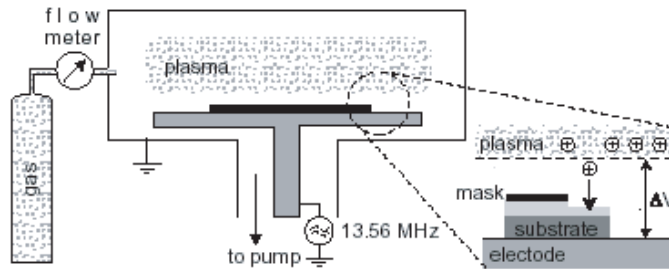


Figure A.1: Scheme of the RIE chamber ( [77])

of this method is that the required time to etch is not limited by the etching of a mask (leading eventually to its removal, and then the loss of selectivity). Recipe for buffered hydrofluoric acid (bHF) is (see [77] or [78]) : 28 ml HF (40%), 170 ml H<sub>2</sub>O, 113 g NH<sub>4</sub>F. It etches with a rate around 70 nm/min.

### A.3 Metal evaporation

In a vacuum chamber, electron coming out of a filament are accelerated over a metal source until its surface melts. The metal evaporates then in all directions, notably on the sample mounted with its surface facing the metal source. Successive evaporation can be made without breaking the vacuum, what is useful if some adhesion layer is needed for example. One can also make some angle evaporation, depending on the requirements of the structure. The thickness of the evaporated material is measured by a calibrated quartz resonator. The chamber used for this work is a PLS 500, from Balzers.

Two actions can improve the adhesion of the evaporated layer: argon sputtering before evaporation and cooling of the sample holder (hence also sample) with liquid nitrogen during evaporation. To run argon sputtering, first a flow of argon is let in the chamber, typically of 4sccm, i.e. the chamber

of the room is around  $10^{-4}$ mbar). Then a sputtering gun ionizes the argon atoms (arc discharge between an anode and cathode) and accelerates them with a grid set at a given voltage. At their exit of the gun, they are neutralized by a warm filament supplying electrons, and then they sputter the sample. Typical control parameters are the current of ionized atoms, the acceleration voltage and the time of the process. For our purpose, parameters have to be soft to avoid etching the resist layer, i.e. the time is in the order of ten of seconds. The advantage of this cleaning method is that there is no brake of vacuum between sputtering and metal evaporation.

## A.4 Example

An example combining all those techniques is shown in Fig.A.2. The detailed procedure to get it is the following:

- A piece of Si(p-doped)-SiO<sub>2</sub>(800 nm)-Si<sub>3</sub>N<sub>4</sub>(210 nm) (2cm\*2cm) is cut and cleaned in organic solvent (acetone, ethanol) in ultrasonic bath for several minutes. Then a drop of PMMA is spun (800 nm thick) and the sample is baked for 30 min at 180°C.
- A first lithography step is done in JEOL where big pads and alignment crosses are designed. Small crosses are written with 50 pA at magnification 1000, i.e. write field size is 100 $\mu$ m\*100 $\mu$ m, and large pads with 45 nA at magnification 25, i.e. write field size is 2mm\*2mm. Developing in MibK/IPA (1/3) for 45 s and stoping in IPA for 30 s.
- Evaporation of 5 nm Ti, 80 nm Au. Lift off.
- Second lithography step : new PMMA, baking, and designing of trench (the big pads and the small crosses are used for a precise alignment). Developing.
- RIE etching (100 W, 34:4 vol ratio of CHF<sub>3</sub>/O<sub>2</sub>, 0.025 mTorr) for 8 min (250 nm are etched).
- Wet etching in bHF (28 ml HF (40%), 170 ml H<sub>2</sub>O, 113 g NH<sub>4</sub>F) for 10min, rinse in DI water (700 nm are etched)

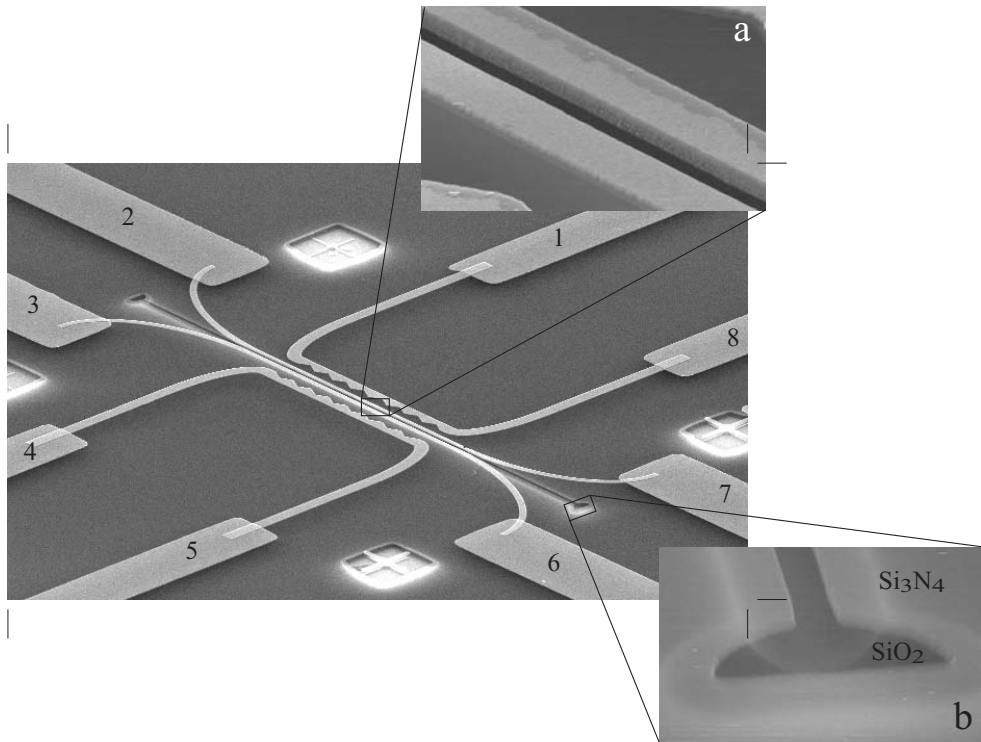


*Figure A.2:* A design combining different structuring techniques presented in this work.  
 a) magnified view of the inner electrodes and trench  
 b) one clearly sees the Si<sub>3</sub>N<sub>4</sub> etched with right angles (RIE) and the underneath SiO<sub>2</sub> etched in a diffuse way (chemical etching) The width of the gap is around 450 nm and its depth around 950 nm.

- Third lithography step : new PMMA, baking, and designing of electrodes around the trench (same parameters as for small crosses), also aligned on crosses. Developing.
- Before evaporation, an Ar-sputtering process (20 mA, 500 V, 10 s) is done in order to really clean the surface. Then evaporation (5 nm Ti, 80 nm Au) is done without breaking vacuum. The substrate is cooled with nitrogen during evaporation. Lift off.



# Appendix B

## Observation Instruments

### B.1 LEEPS

Initial manipulations and electric measurement on DNA were initially performed in the group by Hans-Werner Fink who used a home built instrument called LEEPS microscope (for Low Energy Electron Point Source). As the microscope was only used at the beginning of this work, here are exposed the basics of it (details can be found in [35] or [34]).

A scheme (Fig.B.1) shows the principles of the LEEPS microscope: a source tip (1) that is shaped in an atomic pyramid terminated by just one individual atom sends a coherent wave on the free standing sample (2). At low magnification, the detector (4) just gets a projection image of the sample, and the magnification is determined by the geometry (ratio of the distances). At high magnification, the projection image turns into an hologram, where the unscattered electron form the reference wave. Those in-line holograms can be reconstructed with the help of a computer program (whose principle is to illuminate the hologram with a spherical wave analogous to the radiation used in the experiment). In the experiment described in [35], only the projection image was considered.

To test the electrical conductivity of the DNA, a manipulation tip (3) is used to contact somewhere the free suspended strand. A voltage  $U_m$  is applied and the current is measured. As shown in Fig.B.2, linear I/V curves can be measured (i.e. without gap) with resistances in the order of  $M\Omega$  for 600 nm long rope. The question of whether this low conductivity is due to any artefact is still open. The conduction does not depend whether

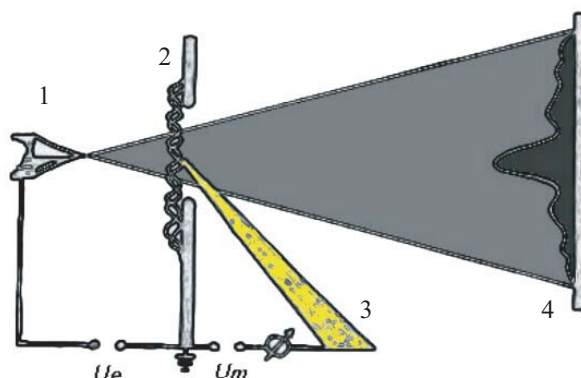
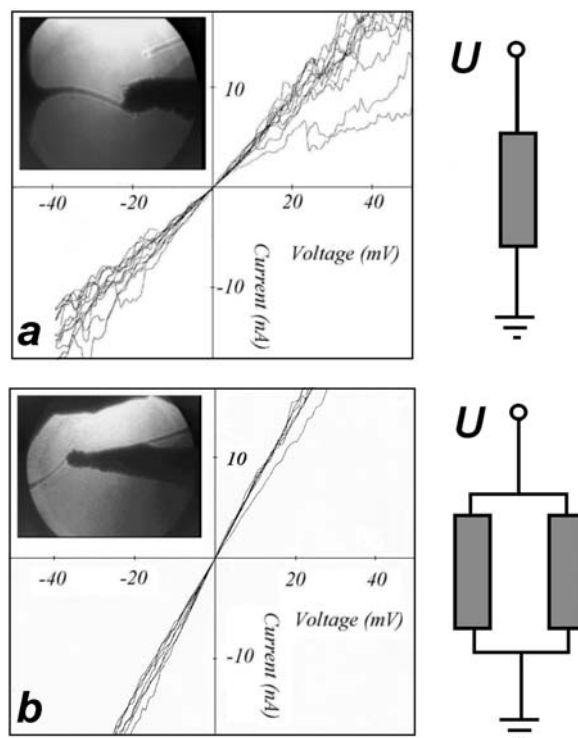


Figure B.1: Scheme of the LEEPS microscope.

the sample is illuminated or not, but as it is not possible to test a sample without first observing it, the effect of the low energy electron beam remains ambiguous. However, if the electron beam had any effect on the DNA, it would be surprising that it is an enhancing of the electrical conductivity.

## B.2 SEM

A scanning electron microscope (SEM) uses as illumination source a beam of electron with energy in the order of 2-30 keV. Several phenomena occur when they hit the sample's surface, but the one used to get a SEM topographic image is the emission of secondary electrons (whose energy is low so the mean free path in the sample is very short, i.e. only those created very close to the surface can escape) that are collected in a detector. The scanning image gives then a picture that looks the same as if a larger sample would be illuminated with light, i.e. giving an image with bright parts and shadows. The SEM microscope is thus a very useful tool to investigate conductive sample. On insulating surface, the electrons deposited by the beam perturb the beam itself, hence the poor resolution: it is then useful to cover previously the surface with a thin metal film. Note that for silicon oxide, that is insulating, the electron from the beam can easily go through the oxide layer and reach the conductive silicon underneath, so that almost no charging effects occur. For this work, a XL30-FEG from Philips was used.



*Figure B.2:* Measuring the DNA rope conductivity in the LEEPS microscope: LEEPS projection image (inset), I/V curves and electrical scheme.

a) The rope has been cut by the tip. The tip contacts now only the left part of it (about 600 nm long). The resistance is roughly  $2.5 \text{ M}\Omega$ .

b) The tip contacts both ropes, so the measured resistance is decreased (roughly a factor two, as depicted by the scheme)

### B.3 Fluorescence microscopy

Luminescence is the emission of light from any substance and occurs from electronically excited states. Depending on the nature of the excited state, two categories are defined: fluorescence and phosphorescence. Fluorescence occurs when the excited electron is in a singlet state (opposite spin to the ground state electron), so the decay is spin-allowed and fast (typically in order of nanoseconds). Phosphorescence happens when the excited electron is in a triplet state (same spin as ground state electron), so the decay is orders of magnitude slower than for fluorescence, typically milliseconds up to seconds.

The processes which occur between the absorption and emission of light are usually illustrated by a Jablonski diagram (Fig.B.3), named after Alexander Jablonski (1898-1980), who is regarded as the father of fluorescence spectroscopy. The singlet ground state, first, and second electronic states are depicted by  $S_0$ ,  $S_1$ , and  $S_2$  respectively. At each of these electronic energy levels fluorophores can exist in a number of vibrational energy levels, denoted by 0, 1, 2, etc. Following light absorption, several processes usually occur. One is called internal conversion: it is the relaxation to the lower vibrational excited state (typically in picoseconds). Then there is the fluorescence itself, with emission of photon (nanoseconds to tens of nanoseconds), or undergoes a spin conversion to a triplet state  $T_1$ , followed by a slow emission of photon, called phosphorescence. The spin conversion is also called intersystem crossing, and it occurs more often with molecules containing heavy atoms (like bromium or iodium). As long as enough energy is given, the emission spectrum of a fluorophore does not depend on the excitation wavelength.

The intensity of the fluorescence can be decreased by several processes, called quenching. Collisional quenching occurs when the excited-state fluorophore is deactivated upon contact with some molecule in solution called quencher. It can lead to non radiative decay to the ground state, electron transfer to the quencher or intersystem crossing to the triplet state<sup>1</sup> (molecular oxygen is a typical quencher via intersystem crossing). Static quenching is the result of formation of non radiative complex between the fluorophore and the quencher. Note that quite often, there is a mixture of the two processes (collisional and static quenching).

---

<sup>1</sup>In fluid solutions the long-lived triplets are completely quenched, so that phosphorescence can not be observed

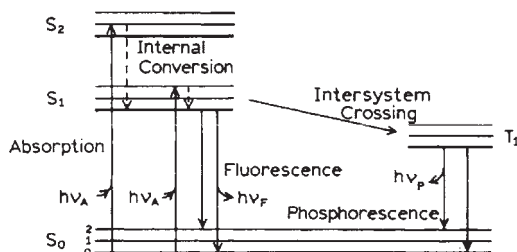
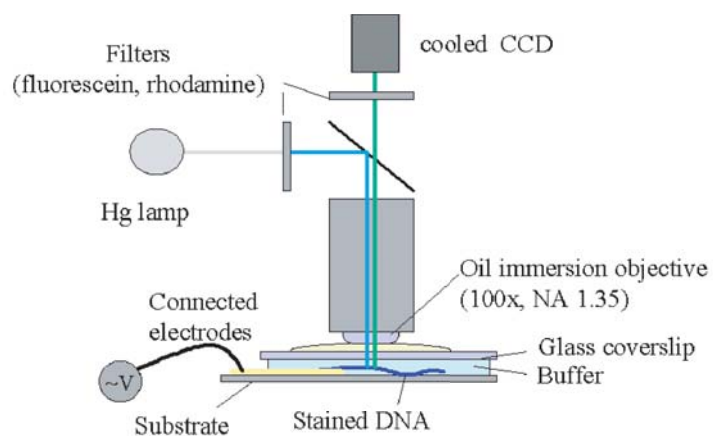


Figure B.3: One form of a Jablonski diagram [73].

Fluorescence can also be suppressed with the presence of a molecule whose absorption spectrum overlaps with the emission spectrum of the fluorophore. Then there is a energy transfer from the fluorophore (donor) to this molecule (acceptor), with a transfer rate proportional to  $\left(\frac{R_0}{r}\right)^6$ , where  $R_0$  is the Förster distance (distance at which resonance energy transfer (RET) is 50% efficient, typically 2 to 6 nm) and  $r$  the distance between donor and acceptor).

Chemists developed a lot of different fluorophore molecules with different absorption and emission spectrum and with different affinities depending on which medium one wants to emphasize. Some of these have been designed to attach to DNA strand: when observed with an optical microscope with the corresponding filters, a good contrast is obtained so that almost only DNA is seen. With good optical properties (high numerical aperture, high magnification of the objective and high intensity light source) single dsDNA can be observed. That clearly emphasizes the power of fluorescence microscopy, since DNA strands are much too small to be resolved with a normal light microscope.

For this work, the images were realized with a fluorescence microscope (BX51 from Olympus) equipped with a 100x/NA1.35 oil immersion objective and a cooled CCD camera (Orca II from Hamamatsu). Two kinds of fluorophores were used: YOYO-1 iodide (491/509) and ethidium homodimer-2 (535/624) from Molecular Probes. Three combinations of filters (Olympus) could be used : U-MWIB2 (BP460-490, BA510-IF, dichroic mirror 505nm) and U-MWIBA2 (BP460-490, BA510-550, dichroic mirror 505nm) for YOYO and U-MWIG2 (BP520-550, BA580-IF, dichroic mirror 565nm) for eth-2 (see Appendix c) for sample preparation. The scheme of the set-up is shown in Fig. B.4 and a picture in Fig. B.5.



*Figure B.4:* Scheme of the observation with fluorescence microscope at the same time as stretching.

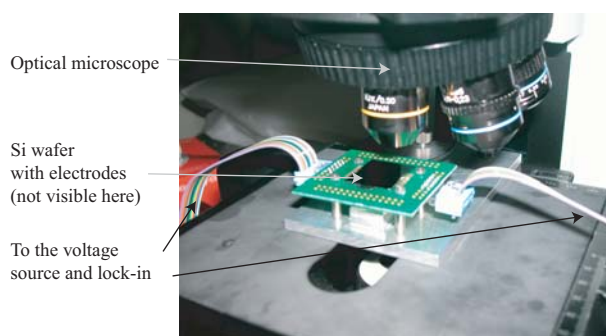


*Figure B.5:* Picture of a sample ready to get DNA.

# Appendix C

## Recipes

### C.1 DNA Fibers

- **Products**

Deoxyribonucleic acid sodium salt from calf thymus, from Sigma, product name: D1501

or

Deoxyribo Nuclear Acid, Sodium Salt, High Molecular Weight Kalbthymus, from MERCK, Art. 24706

- **Solution**

Dionized water (18M $\Omega$ cm), or TRIS 10mM- EDTA 1mM and different salt concentration

### C.2 Hydrodynamic stretching

- **Products**

$\lambda$ -DNA from bacteriophage lambda, from Roche, product number: 745782

250 $\mu$ g/ml in TE pH 8.0, 48502 bp

- **Solution**

TRIS 10mM-EDTA 1mM buffer, 1 to 10 mM NaCl, pH 7 to 9 (adjusted with HCL or NaOH)

1 to 10 $\mu$ g/ml of  $\lambda$ -DNA in buffer solution

### C.3 Electric-field

- **Products**

same lambda DNA as for hydrodynamic stretching

- **Solution**

MES buffer, pH 4.1, conductivity  $\sigma = 70\mu S/cm$

1 $\mu g/ml$  of  $\lambda$ -DNA in buffer solution

- **Other DNA**

Those DNA were prepared by Dr. Nikolay Korolev, Division of Physical Chemistry, Stockholm University

Na-DNA or Mg-DNA from salmon testes from Fluka BioChemika, product number: 31363

Na-DNA or Mg-DNA from calf thymus, ultra pure, separated by Prof. D. Y. Lando, Institute of Bioorganic chemistry, Belorussian Academy of Science, Minsk

To separate Na-DNA, ultrafiltration procedure was carried out three times by washing the DNA solution with 50mM NaCl, 1mM Na<sub>2</sub>EDTA. To exchange Na<sup>+</sup> for Mg<sup>2+</sup>, stock DNA solutions were washed five times with 50mM MgCl<sub>2</sub>.

### C.4 Staining

- **Prestaining:** A solution with a ratio of 10<sup>4</sup> dye molecules per  $\lambda$ -DNA strand, i.e. 1 dye molecule per 5 bp, is prepared.

The dye used is YOYO-1, from molecular probes (Y-3601). Its molecular weight is 1270.65 D.

- **Counterstaining:** A solution of few nM dye solution in PBS is prepared. 100  $\mu l$  of the dye solution are applied to the substrate with DNA in let incubate for 20 min at room temperature. The sample is then gently rinsed with deionized water.

The dye used is Ethidium homodimer-2, from molecular probes (E-3599), in a stock concentration of 1mM in DMSO.

# Bibliography

- [1] R. P. Feynman, There's plenty of room at the bottom, <http://www.zyvex.com/namynotech/feynman.html>.
- [2] C. Joachim, J. K. Gimzewski, and A. Aviram, *Electronics using hybrid-molecular and mono-molecular devices*, Nature **408**, 541 (2000).
- [3] R. F. Service, *Molecules get wired*, Science **294**, 2442 (2001).
- [4] <http://www.lab-on-a-chip.com/home/index.html>.
- [5] B. Joy, *Why the future doesn't need us*, Wired **April** (2000).
- [6] P. J. Dandliker, R. E. Holmlin, and J. K. Barton, *Oxidative thymine dimer repair in the DNA helix*, Science **275**, 1465 (1997).
- [7] A. Aviram and M. Ratner, *Molecular rectifiers*, Chem. Phys. Lett. **29**, 277 (1974).
- [8] B. Alberts et al., *Molecular Biology of the Cell*, Garland Publishing, 1994.
- [9] L. M. Adleman, *Molecular computation of solutions to combinatorial problems*, Science **266**, 1021 (1994).
- [10] Y. Benenson et al., *Programmable and autonomous computing machine made of biomolecules*, Nature **414**, 430 (2001).
- [11] J. Fritz et al., *Translating biomolecular recognition into nanomechanics*, Science **288**, 316 (2000).
- [12] J. Chen and N. C. Seeman, *Synthesis from DNA of a molecule with the connectivity of a cube*, Nature **350**, 631 (1991).
- [13] Y. Maeda et al., *Controlled conjugation of nanoparticles with single stranded DNA*, J. Vac. Sci. Technol. B **17**, 494 (1999).

- 
- [14] E. Braun, Y. Eichen, U. Sivan, and G. Ben-Yoseph, *DNA templated assembly and electrode attachment of a conducting silver wire*, Nature **391**, 775 (1998).
- [15] J. Richter, M. Mertig, W. Pompe, I. Mnch, and H. K. Schackert, *Construction of highly conductive nanowires on a DNA template*, Appl. Phys. Lett. **78**, 536 (2001).
- [16] J. K. N. Mbindyo et al., *DNA directed assembly of gold nanowires on complementary surfaces*, Adv. Mater. **13**, 249 (2001).
- [17] W. E. Ford, O. Harnack, A. Yasuda, and J. M. Wessels, *Platined DNA as precursors to templated chains of metal nanoparticles*, Adv. Mater. **13**, 1793 (2001).
- [18] J. Jortner, M. Bixon, T. Langenbacher, and M. E. Michel-Beyerle, *Charge transfer and transport in DNA*, Proc. Natl. Acad. Sci. USA, Chemistry **95**, 12759 (1998).
- [19] M. R. Arkin et al., *Rates of DNA mediated electron transfer between metal-lointercalators*, Science **273**, 475 (1996).
- [20] F. D. Lewis et al., *Distance dependent electron transfer in DNA hairpins*, Science **277**, 673 (1997).
- [21] S. Priyadarshy, S. M. Risser, and D. N. Beratan, *DNA mediated electron transfer*, Journ. of Biol. Inorg. Chem. **3**, 196 (1998).
- [22] C. Wan et al., *Femtosecond dynamics of DNA mediated electron transfer*, Proc. Natl. Acad. Sci. USA, Chemistry **96**, 6014 (1999).
- [23] B. Giese, J. Amaudrut, A. Khler, M. Spormann, and S. Wessely, *Direct observation of hole transfer through DNA by hopping between adenine bases and by tunneling*, Nature **412**, 318 (2001).
- [24] S. Roth, *One-dimensional metals*, VCH Weinheim, 1995.
- [25] N. F. Mott and E. A. Davis, *Electronic processes in non-crystalline materials*, Clarendon press, Oxford, 1979.
- [26] D. D. Eley and D. I. Spivey, *Semiconductivity of Organic Substances*, Trans. Faraday Soc. **58**, 411 (1962).
- [27] R. S. Snart, *The electrical properties and stability of DNA to UV radiation and aromatic hydrocarbons*, Biopolymers **12**, 1493 (1973).

- 
- [28] P. Tran, B. Alavi, and G. Grüner, *Charge transport along the lambda DNA double helix*, Phys. Rev. Lett. **85**, 1564 (2001).
- [29] G. Grüner, *Millimeter and submillimeter wave spectroscopy of solids*, volume 74 of *Topics in applied physics*, pages 111–168, Springer, 1998.
- [30] C. R. Cantor and P. R. Schimmel, *Biophysical Chemistry*, W. H. Freeman and company, 1980.
- [31] J. M. Warman, M. P. de Haas, and A. Rupprecht, *DNA : a molecular wire ?*, Chem. Phys. Lett. **249**, 319 (1996).
- [32] R. Guckenberger et al., *Scanning tunneling microscopy of insulators and biological specimens based on lateral conductivity of ultrathin water films*, Science **266**, 1538 (1994).
- [33] M. Furukawa, H. Tanaka, and T. Kawai, *The role of dimer formation in the self-assemblies of DNA base molecules on Cu111 surfaces : a scanning tunneling microscope study*, Science **115**, 3419 (2001).
- [34] H.-W. Fink, W. Stocker, and H. Schmid, *Holography with Low-Energy Electrons*, Phys. Rev. Lett. **70**, 2679 (1990).
- [35] H.-W. Fink and C. Schönenberger, *Electrical conduction through DNA molecules*, Nature **398**, 407 (1999).
- [36] P. J. de Pablo et al., *Absence of DC-conductivity in lambda DNA*, Phys. Rev. Lett. **85**, 4992 (2000).
- [37] L. Cai, H. Tabata, and T. Kawai, *Self assembled DNA networks and their electrical conductivity*, Appl. Phys. Lett. **77**, 3105 (2000).
- [38] K. H. Yoo et al., *Electrical conduction through poly(dA)-poly(dT) and poly(dG)-poly(dC) DNA molecules*, Phys. Rev. Lett. **87**, 198102 (2001).
- [39] D. Porath, A. Bezryadin, S. de Vries, and C. Dekker, *Direct measurement of electrical transport through DNA molecules*, Nature **403**, 635 (2000).
- [40] A. J. Storm, J. van Noort, S. D. Vries, and C. Dekker, *Insulating behavior for DNA molecules between nanoelectrodes at the 100 nm length scale*, Appl. Phys. Lett. **79**, 3881 (2001).
- [41] A. Y. Kasumov et al., *Self assembled DNA networks and their electrical conductivity*, Science **291**, 280 (2001).

- 
- [42] M. Krüger, *Towards single molecule electronics*, PhD thesis, University of Basel, 2000.
- [43] T. Kunugi and H. Okuzaki, *Electrical and mechanical properties of the zone-drawn polypyrrole films*, Journal of Polymer Science B **34**, 1269 (1996).
- [44] Y. Okahata, T. Kabayashi, K. Tanaka, and M. Shimomura, *Anisotropic electric conductivity in an aligned DNA cast film*, J. Am. Chem. Soc. **120**, 6165 (1998).
- [45] H. Nakayama, H. Ohno, and Y. Okahata, *Intramolecular electron conduction along DNA strands and their temperature dependency in a DNA aligned cast film*, Chem. Commun. , 2300 (2001).
- [46] G. Hartwich et al., *Electrochemical study of electron transport through thin DNA films*, J. Am. Chem. Soc. **121**, 10803 (1999).
- [47] A. Meister, *Elektrische leitfähigkeit von desoxyribonukleinsäure*, Master's thesis, University of Basel, 2001.
- [48] M. C. Petty, M. R. Bryce, and D. Bloor, *Introduction to molecular electronics*, Oxford University Press, 1995.
- [49] L. McFail-Isom, X. Shui, and L. D. Williams, *Divalent Cations Stabilize Unstacked Conformations of DNA and RNA by Interacting with Base Pi Systems*, Biochemistry **37**, 17105 (1998).
- [50] D. R. Lide, *Handbook of Chemistry and Physics*, CRC Press, 1994.
- [51] R. H. Austin, J. P. Brody, E. C. Cox, T. Duke, and W. Volkmuth, *Stretch genes*, Physics Today , 32 (1997).
- [52] P. J. Hagerman, *Flexibility of DNA*, Ann. Ref. Biophys. Biophys. Chem. **17**, 265 (1988).
- [53] P. Cluzel et al., *DNA: an extensible molecule*, Science **271**, 792 (1996).
- [54] M. E. Hogan and R. H. Austin, *Importance of DNA stiffness in protein-DNA binding specificity*, Nature **329**, 263 (1987).
- [55] Y. Arai et al., *Tying a molecular knot with optical tweezers*, Nature **399**, 446 (1999).
- [56] S. R. Quake, H. Babcock, and S. Chu, *The dynamics of partially extended single molecules of DNA*, Nature **388**, 151 (1997).

- 
- [57] T. T. Perkins, S. R. Quake, D. E. Smith, and S. Chu, *Relaxation of a single DNA molecule observed by optical microscopy*, Science **264**, 822 (1994).
- [58] A. Bensimon et al., *Alignment and sensitive detection of DNA by a moving interface*, Science **265**, 2096 (1994).
- [59] J. H. Moon, J. W. Shin, S. Y. Kim, and J. W. Park, "Formation of uniform aminosilane thin layers : an imine formation to measure relative surface density of the amine group", Langmuir **12**, 4621 (1996).
- [60] K. H. Choi et al., *Controlled deposition of CNT on a patterned substrate*, Surface Science **462**, 195 (2000).
- [61] P. S. Doyle, B. Ladoux, and J.-L. Viovy, *Dynamics of a tethered polymer in shear flow*, Phys. Rev. Lett. **84**, 4769 (2000).
- [62] D. Bensimon, A. J. Simon, V. Croquette, and A. Bensimon, *Stretching DNA with a receding meniscus : experiments and models*, Phys. Rev. Lett. **74**, 4755 (1995).
- [63] C. Rivetti, M. Guthold, and C. Bustamante, *Scanning Force Microscopy of DNA deposited onto Mica*, J. Mol. Biol. **264**, 919 (1996).
- [64] R. M. Zimmermann and E. C. Cox, *DNA stretching on functionalized gold surfaces*, Nucleic Acid Research **22**, 492 (1994).
- [65] M. Washizu and O. Kurosawa, *Electrostatic manipulation of DNA in micro-fabricated structures*, IEEE Transactions on industry applications **26**, 1165 (1990).
- [66] C. L. Asbury and G. van der Engh, *Trapping of DNA in nonuniform oscillating electric fields*, Biophysical Journal **74**, 1024 (1998).
- [67] H. A. Pohl, *Dielectrophoresis*, Cambridge university press, 1978.
- [68] R. Pethig, *Dielectric and electronic properties of biological materials*, John Wiley and Sons, 1978.
- [69] S. Takashima, *Electrical Properties of Biopolymers and Membranes*, Adam Hilger, 1989.
- [70] M. Washizu, O. Kurosawa, I. Arai, S. Suzuki, and N. Shimamoto, *Applications of electrostatic stretch and positioning of DNA*, IEEE Transactions on industry applications **31**, 447 (1995).

- 
- [71] A. Bachtold, *Electrical properties of single multiwalled carbon nanotubes*, PhD thesis, University of Basel, 1999.
- [72] X. D. Cui et al., *Reproducible measurement of single-molecule conductivity*, *Science* **294**, 571 (2001).
- [73] J. R. Lakowicz, *Principles of Fluorescence Spectroscopy*, Kluwer Academic, 1999.
- [74] Y. Zhang, R. H. Austin, J. Kraeft, E. C. Cox, and N. P. Ong, *Insulating behavior of  $\lambda$ -DNA on the micron scale*, arXiv:physics/0205016 (2002).
- [75] M. Bockrath et al., *Scanned conductance microscopy of carbon nanotubes and  $\lambda$ -DNA*, *Nanoletters* **2**, 187 (2002).
- [76] A. Rakitin et al., *Metallic conduction through engineered DNA: DNA nano-electronic building blocks*, *Phys. Rev. Lett.* **86**, 3870 (2001).
- [77] T. Hoss, *Electronic Transport and Noise in Mesoscopic SNS/SFS-junctions*, PhD thesis, University of Basel, 2000.
- [78] S. M. Sze, *Physics of Semiconductor Devices*, John Wiley and Sons, 1981.

# Publication list

## Publications in journals and proceedings:

- *DNA: An electrical conductor?*, C. Schönenberger, F. Dewarrat, M. Calame, K. Furukawa and H.-W. Fink, Int. Conf. on Molecular Electronics and Bioelectronics, Awaji Japan (2001) .
- *Orientation and Positioning of DNA Molecules with an Electric Field*, F. Dewarrat, M. Calame and C. Schönenberger, Single Mol.**3**, 189 (2002).
- *Insulating behavior of DNA*, (to be published).

## Talks

- *Electric conductivity of DNA*, Short presentation at the VIII Summer School Nicolas Cabrera "Where Physics and Biology meet", 17-21 September 2001, Madrid, Spain.
- *Positioning of DNA molecules over electrodes using an electrical field based technique*, IV. Annual Linz Winterworkshop, "Single Molecule Techniques in Biophysics and Drug Discovery", 1-4 February 2002, Linz, Austria.
- *Manipulations of DNA molecules and electrical characterization*, Meeting of the Swiss Physical Society, 28-29 February 2002, Lausanne, Switzerland.

## Poster contributions

- *Electrical conductivity of DNA*, F. Dewarrat, H.-W. Fink, and

C. Schönenberger, TMR Network School, 25-29 May 1999, Bad Herrenalb, Germany.

- *Towards DNA's electrical conductivity measurements*, F. Dewarrat, K. Furukawa, M. Calame, and C. Schönenberger, 4th Hasliberg Workshop on Nanoscience, 16-20 October 2000, Hasliberg, Switzerland.
- *Wire-Like Molecules as Electrical Conductors*, A. Bachtold, D. Babić, M. Buitelaar, F. Dewarrat, M. Calame, H.-W. Fink, K. Furukawa, M. Iqbal, M. Krüger, T. Nussbaumer, C. Strunk, C. Schönenberger, and C. Terrier, Poster at the Closing meeting of the NFP36 National Science Program on Nanoscience, 14 November 2000, Bern, Switzerland.
- *Electrical conductivity investigations on DNA*, F. Dewarrat, K. Furukawa, M. Calame, and C. Schönenberger, 7th MEL-ARI/NID Workshop, 7-9 February 2001, Barcelona, Spain.
- *Electrical transport investigations in DNA single molecules and fibers*, M. Calame, F. Dewarrat, A. Meister, K. Furukawa, and C. Schönenberger, Electronic Interaction Electron Dynamics in DNA, 4-8 September 2001, Los Angeles, USA.
- *DNA molecules manipulations and electrical characterization. From Solid State to Biophysics*, M. Calame, F. Dewarrat, and C. Schönenberger, Cavtat, 12-19 June 2002, Dubrovnik, Croatia.
- *Growth and Functionalization of Carbon Nanotubes Arrays: a step towards new biomolecular recognition techniques* Z. Liu, M. Calame, F. Dewarrat, S. Ifadir, and C. Schönenberger, NCCR Nanoscale Science Workshop, 3-6 September 2002, Pontresina, Switzerland.

# Curriculum Vitae

François Dewarrat

19. 7. 1974      Born in Billens, Switzerland
- 1980 - 1989      Elementary school in Fribourg and Bulle
- 1989 - 1993      Swiss maturity type A (latin-greek)
- 1993 - 1998      Physics studies at the University of Fribourg  
Experimental physics, theoretical physics and mathematics
- 1998              Diploma work in experimental solid state physics  
in the group of Prof. Louis Schlapbach  
"Dépôts de carbone par électrochimie  
et de nanodiamants par électrophorèse"
- 1998              Stay of two months in the group of Prof. Dag Noreus  
Institute of chemistry, Stockholm University, Sweden.
- 1998 - 2002      Phd studies at the University of Basel  
in the group of Prof. Christian Schönenberger  
Assistant in practice for beginner and first year physics exercise
- 2001              Stay of 5 weeks in the basic research laboratory of NTT  
Atsugi, Japan
28. 6. 2002      Thesis Defense

**I thank the following professors for my scientific education:**

X. Bader, D. Baeriswyl, X. Bagnoud, J.-C. Dousse, R. Ingold, P. Junod, B. Kaup, J. Kern, H. Kleisli, R. Kunz, L. Schaller, L. Schlapbach, L. Schellenberg, C. Schönenberger, H. Schneuwly, Y.-C. Zang

# Remerciements

C'est avec plaisir que je remercie ici tout d'abord mon professeur de thèse Christian Schönenberger qui m'a dirigé durant toute cette période. J'espère que ses compétences scientifiques m'auront été bénéfiques au maximum et que je saurai plus tard me souvenir de tous ses enseignements. Ce que je suis sûr de ne pas oublier par contre, c'est son enthousiasme communicatif et sa grande disponibilité, que ce soit pour des discussions de point de vue ou des explications pratiques dans le laboratoire. Je remercie aussi très chaleureusement Michel Calame qui m'a été d'une aide précieuse dans la réalisation des expériences, dans leurs interprétations et dans la formulation des résultats. J'adresse aussi un merci tout particulier à Kazuaki Furukawa, qui a passé six mois avec nous à Bâle et grâce à qui j'ai pu aller moi-même cinq semaines mener quelques compléments d'expériences au laboratoire NTT dans la banlieue de Tokyo. Ce fut pour moi l'occasion d'appréhender un environnement de travail et de vie bien différent, ce dont je garde un excellent souvenir: *domo arigato gozaimas'*.

Je remercie encore les autres membres, anciens et actuels, du groupe de physique mésoscopique qui m'ont aussi, à un moment ou à un autre, donné un coup de main: Bakir Babić, Dinko Babić, Adrian Bachtold, Mark Buitelaar, Bong-Ryoul Choi, Shadyar Fahrangfar, Jürg Furer, Matthias Gräber, Lucia Grüter, Adam Hansen, Tilman Hoss, Soufiane Ifadir, Mahdi Iqbal, Derek Kelly, Takis Kontos, Michael Krüger, Zuqin Liu, Thomas Nussbaumer, Stefan Oberholzer, Sangeeta Sahoo, Christoph Strunk, Christophe Terrier. Un clin d'oeil particulier encore à notre diplomant André Meister, chaleureux et enthousiaste, et au professeur Hans-Werner Fink, grâce à qui cette expérience a été lancée. Un grand merci aussi à Martin Hegner pour son aide avec le microscope AFM et ses conseils généraux concernant l'ADN.

Je remercie enfin ceux qui m'ont aidé d'un peu plus loin, comme les secrétaires de l'Institut Astrid Kalt et Barbara Kammerman, des membres de

